Use of microfluidic experiments to optimize MICP treatment protocols for effective strength enhancement of MICP-treated sandy soils

Yuze Wang[1,2] · Charalampos Konstantinou[3] · Kenichi Soga[4] · Giovanna Biscontin[5] · Alexandre J. Kabla[5]

Abstract

Microbially induced calcium carbonate ($CaCO_3$) precipitation (MICP) has been extensively studied for soil improvement in geotechnical engineering. The quantity and size of calcium carbonate crystals affect the strength of MICP-treated soil. In this study, microfluidic chip experiments and soil column experiments were conducted to optimize MICP treatment protocols for effective strength enhancement of MICP-treated sandy soils. The microscale experiments reveal that, due to Ostwald ripening, longer injection intervals allow crystals to dissolve and reprecipitate into larger crystals regardless of the concentration of cementation solution. Even though a cementation solution input rate of 0.042 mol/l/h is sufficient to maintain a high chemical transformation efficiency, a further reduction in the input rate by about four times resulted in an increase in the size of crystals produced by the end of treatment from about 40 to 60 μm. These findings were applied in soil column experiments. Results showed that significantly larger crystals and higher soil strength were achieved when the normalized rate of cementation solution injection was reduced from 0.042 to 0.021 mol/l/h. Crystal size and soil strength increased slightly more when the normalized input rate was further reduced from 0.021 to 0.010 mol/l/h. This study demonstrates how data from microscale microfluidic experiments that examine the effects of injection intervals and concentration of cementation solution on the properties of calcium carbonate crystals can be used to optimize MICP treatment in macroscale sand soil column experiments for effective strength enhancement.

Keywords Microbially induced calcium carbonate ($CaCO_3$) precipitation (MICP) · Microfluidics · Microscale properties · MICP optimization · Strength enhancement

✉ Yuze Wang
  wangyz@sustech.edu.cn

1 Southern Marine Science and Engineering Guangdong Laboratory (Guangzhou), Shenzhen, China

2 Department of Ocean Science and Engineering, Southern University of Science and Technology, Shenzhen, China

3 Department of Civil and Environmental Engineering, University of Cyprus, Nicosia, Cyprus

4 Department of Civil and Environmental Engineering, University of California, Berkeley, USA

5 Department of Engineering, University of Cambridge, Cambridge, UK

1 Introduction

Bio-cementation techniques, including microbially induced carbonate precipitation (MICP) and enzyme-induced carbonate precipitation (EICP), have been introduced in recent years for cementing geological formations such as soils and fractured rocks by using biofluids and chemical solutions to induce carbonate precipitation, thereby cementing geological formations [6, 7, 11–13, 16, 19, 23, 26, 30, 31]. Due to its ease of control and high chemical transformation efficiency, ureolysis-driven MICP is among the most studied MICP processes [14]. During a ureolysis-driven MICP treatment procedure aiming to increase soil strength or to alter soil permeability, ureolytic bacterial suspension (biofluid) is injected into soil, after which a few hours are given for the bacterial cells to settle and attach to soil particle surfaces before cementation solution (which

mainly contains urea and CaCl$_2$) is injected into the soil matrix multiple times. The bacteria hydrolyse urea, producing CO_3^{2-}, which reacts with Ca^{2+} to form $CaCO_3$ (Eqs. 1 and 2). The precipitated $CaCO_3$ bonds soil particles, increases the strength of soil matrices and alters soil permeability.

$$CO(NH_2)_2 + 2H_2O \xrightarrow{\text{Urease}} 2NH_4^+ + CO_3^{2-} \tag{1}$$

$$Ca^{2+} + CO_3^{2-} \rightarrow CaCO_3(s) \tag{2}$$

Compared to traditional cement, the biofluids which are injected into soil pores or rock fractures have lower viscosities, thus enabling their injection over larger distances, as well as their penetration into smaller fractures [26]. In addition, $CaCO_3$ is also more environmentally friendly compared to cement. However, there are still challenges to overcome before MICP can be widely used in real engineering applications. The bio-geo-chemical processes involved in this technique are complex, making it challenging to control and predict the engineering performance of MICP-treated soils at the macroscale, especially under real environmental conditions. For engineering applications, MICP treatment efficiency needs to be improved significantly in order to become economically viable. Studies have shown that the effectiveness of MICP for soil strength enhancement is affected by properties of $CaCO_3$ crystals and the chemical transformation efficiency, the latter of which affects the calcium carbonate content in treated soils [4, 5, 9].

To overcome the challenges, experimental studies have been conducted to understand the process of MICP and to optimize the treatment protocols. In addition, numerical simulations of MICP have also been developed to link the experiments of MICP to field-scale MICP performance. Soil column experiments, which combine carbonate content testing, unconfined compressive strength testing and/or scanning electron microscopy imaging, have been widely conducted as one of the main methods used for studying MICP. The factors and experimental conditions affecting MICP that have been studied include saturation of soil samples [8], bacterial density, reaction time and curing condition [42], particle size distribution [24], pH [10], and concentration of cementation solution [22, 42].

In recent years, microfluidic chip experiments have become popular for studying the microscale properties of MICP due to the fact that the *in-situ* behaviour of bacteria and calcium carbonate during MICP treatment can be observed and investigated [32]. A microfluidic chip enables the manipulation of small amounts of fluid [38] and can replicate key features of the porous matrix of sandy soil such as the shape irregularity of sand grains and pores, as well as the surface properties of the porous channel [32]. By performing microfluidic chip experiments, MICP has been further explored in terms of microscale processes [17, 33], MICP precipitation kinetics [17, 39, 35], microscale changes with pH variations during MICP treatment [41], and the role of bacteria in MICP and its effects on MICP processes and kinetics [35]. In addition, microfluidic chip experiments have also been used for studying EICP [17, 36, 40]. Unlike core-scale or model-scale soil experiments, microfluidic chip experiments are capable of observing bacterial behaviour and monitoring the whole precipitation processes of calcium carbonate in the porous medium under conditions that mimic the flow conditions in the soil matrix. This provides an opportunity to further explore the microscale mechanisms of MICP or EICP, which will help to advance the understanding the of engineering behaviours of MICP-treated soils.

However, the porous media in microfluidic chips are normally two-dimensional structures, with the third dimension having the same thickness made using polydimethylsiloxane (PDMS), which does not fully replicate the three-dimensional features and surface properties of the porous media of soils such as silicon sands. Therefore, the optimized protocols obtained using microfluidic and soil column experimental methods may be different. Since there are not any previous studies that explore the link between these two types of experiments, the primary objective of this study is to compare the similarities and differences between the optimized MICP protocols at the two scales. To link these two experiments, the MICP treatment procedures conducted in these two experiments both use staged-injection procedures, which involve injecting bacterial suspension, after which the bacteria are given several hours to settle and attach to the porous medium prior to applying any subsequent injections of cementation solution. The work presented herein shows the relationship between these two types of experiments and demonstrates how data from microscale microfluidic experiments can be used to enhance the understanding of MICP microscale mechanisms and thereby optimize the MICP treatment of macroscale sand soil samples for effective strength enhancement.

2 Materials and methods

2.1 Microscale MICP experiments using microfluidic chips

2.1.1 Experimental set-up

As described in [32, 33], a microfluidic chip containing porous channels, made based on a modified cross-sectional image of real sandy soils, is a useful tool to study microscale MICP processes. Figure 1a shows the schematic of the set-up for microfluidic chip experiments, which
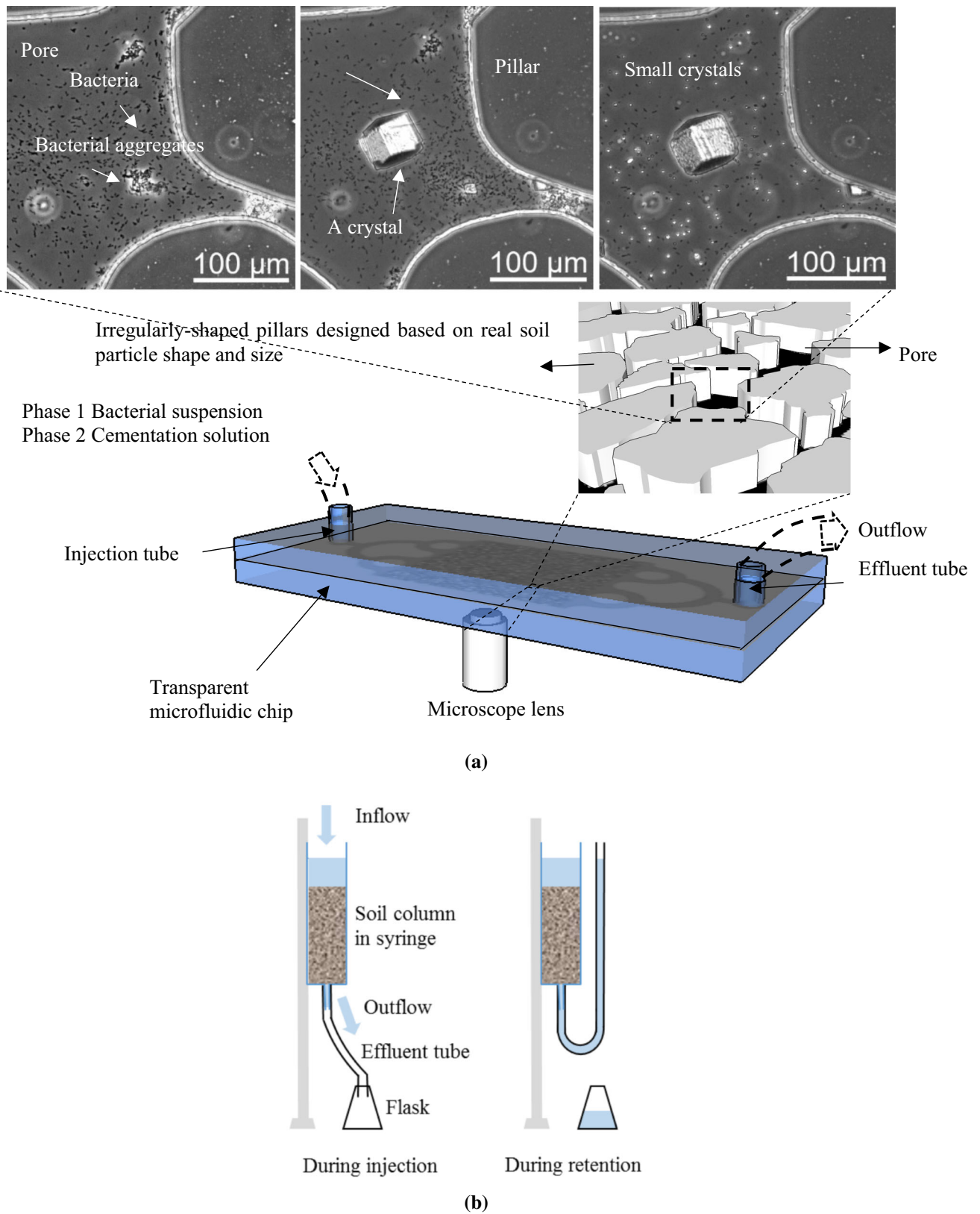
Fig. 1 Schematic of experimental set-up. **a** Microscale microfluidic chip experiments [redrawn based on 32], **b** macroscale soil column experiments (redrawn based on [5])

includes a microfluidic chip, a microscope and a flow injection system consisting of a syringe, a pump and tubing (syringe and pump not shown). The design and fabrication of the microfluidic chip, as well as the detailed imaging technique, are described in Wang et al. [32]. The microfluidic chip experiment was used to observe the formation of calcium carbonate crystals over time during MICP processes involving multiple injections of cementation solution. Magnified images from previous work [33] are shown in Fig. 1a to help identify the microfluidic chip channels, bacteria and crystals.

2.1.2 Bacterial medium and cementation solution

In the microscale experiment conducted in this study, *Sporosarcina pasteurii* (DSM 33) bacterial suspension was cultivated from a frozen stock purchased from Leibniz Institute DSMZ German Collection of Microorganisms and Cell Cultures GmbH (Braunschweig, Germany) following the same procedure as described in [33] until its optical density measured at a wavelength of 600 nm (OD_{600}) reached about 1.0. The ureolysis rate of bacteria was determined using the conductivity method described by Whiffin et al. [37]. The cementation solution contains $CaCl_2$, urea and nutrient broth. The concentrations of $CaCl_2$ and urea varied in different protocols, with either 0.25 M, 0.5 M or 1.0 M $CaCl_2$ together with a 1.5-fold higher concentration of urea being used in each case. In all the protocols, the concentration of nutrient broth is kept constant at 3 g/L. The concentration of urea was 1.5 times higher than the concentration of $CaCl_2$ to ensure efficient calcium transformation [25], and the nutrient broth is used to provide nutrients for bacterial cells to maintain their relatively high activity during the injection of cementation solution.

2.1.3 MICP treatment procedure

After bacterial suspension, cementation solution and microfluidic chips were prepared, a staged-injection MICP process was applied. Four protocols were tested in total

Table 1 Parameters of microfluidic chip experiments

Protocol No.	Chemical concentration	Retention time (h)	Normalized input rate (mole/l per h)
M1	0.25 M Calcium chloride	3–5	0.042
M2	0.25 M Calcium chloride	24	0.010
M3	0.5 M Calcium chloride	24	0.021
M4	1.0 M Calcium chloride	24	0.042

(Table 1). In all of the protocols, after the microfluidic chips were saturated with deionized water, 1.25 pore volumes (PVs) of *Sporosarcina pasteurii* (DSM 33) suspension with an OD_{600} of 1.0 and a bacterial activity of 559.0 ± 27.9 mM/h/OD were injected into the microfluidic chips, after which the bacteria were left to attach to the surface of the microfluidic chip channels for approximately 24 h. Subsequently, multiple injections of 1.25 PVs of cementation solution at different concentrations and injection intervals (retention time) were applied (see Table 1). The injection flow rates of bacterial suspension and cementation solution were 56 PV/h and 5.6 PV/h, which corresponded to Darcy's velocity of 4.6×10^{-4} m/s and 4.6×10^{-5} m/s, respectively. All of the microfluidic chip experiments were conducted at a room temperature of about 20 °C. Protocols M1 and M2 were used to compare the precipitation process when the retention period was 3–5 h compared to 24 h, with the concentration of $CaCl_2$ being the same in both protocols. In each of these two protocols, 3.0 M × 1.2 pore volumes of $CaCl_2$ were injected. Protocols M3 and M4 were used to compare with Protocol M2 to investigate the difference in the $CaCO_3$ precipitation process when the concentration of cementation solution is varied.

2.1.4 Imaging and image analysis

Imaging of the $CaCO_3$ precipitation procedure in the different protocols was achieved using an Axio Observer Z1 research microscope with phase field illumination and 10× inverted objectives to obtain images with a resolution of 0·65 μm/pixel. Detailed parameters of the microscope are described in Wang et al. [32]. Images were taken after the end of each retention period after cementation solution injection to analyse the $CaCO_3$ precipitation process in the different protocols.

To quantify the sizes and volumes of crystals in the images, the diameters of each of the crystals in selected areas of the images were measured, and crystal volumes were calculated based on the assumption that the crystals were half-spheres [17, 33]. To quantify the number of crystals per unit volume, the numbers of crystals in selected areas of the images were counted, and the number obtained was divided by the corresponding void volume of the microfluidic chip channels (V_v), which was calculated by multiplying the depth of microfluidic chip channels (50 μM) by the area of the selected images. To quantify the total amount of crystals, the total volume of the crystals in selected areas of the images V_c and the corresponding void volume of the channels V_v were obtained first and then V_c / V_v was calculated to determine the normalized crystal volume. Assuming that 100% of Ca^{2+} ions transform into $CaCO_3$, the V_c / V_v, denoted as $V_{c100\%}/V_v$, can be calculated as

$$\frac{V_{c100\%}}{V_v} = \frac{[Ca^{2+}] \times IN \times 100\,g/mol}{2.71\,g/cm^3} \times 100\% \qquad (3)$$

where $[Ca^{2+}]$ is the concentration of Ca^{2+} in the cementation solution in mol/L and IN is the number of cementation solution injections. Based on the above equation, the chemical transform efficiency (CTE) is calculated using the following formula:

$$CTE = \frac{\frac{V_c}{V_v}}{\frac{V_{c100\%}}{V_v}} \times 100\% = \frac{V_c}{V_{c100\%}} \times 100\%. \qquad (4)$$

2.2 Macroscale MICP experiments

2.2.1 Sand and sample preparation

Macroscale MICP experiments were conducted using the same set-up as described by Al Qabany and Soga [4]. The schematic of the experiment is shown in Fig. 1b. Syringes with a length of 120 mm and a diameter of 35.4 mm were filled with sand. The granular material was the same as in [4, 5], which is poorly graded sub-rounded sand with a D_{10} value of 165 μm, a D_{90} of 250 μm and specific gravity of 2.65. Each column was filled with 180 g of sand and was vibrated to achieve a final density of 1.65 g/cm^3 and a porosity of about 0.37.

After the sand was placed in the columns and saturated with deionized water, injections of bacterial suspension and cementation solution were performed from top to bottom of the soil columns via gravity using the same staged-injection procedure as in the microfluidic chip experiments. The bacteria, cultivation procedure, specific activity and retention period were kept the same as described in the microscale microfluidic chip experiment. In addition, cementation solution content, ratio of urea to $CaCl_2$ and nutrient broth concentration were also the same as in the microfluidic chip experiments. 1.2 PV of bacterial suspension or cementation solution was injected in each injection to ensure that all of the soil pores were replaced with a new batch of cementation solution and to ensure that the liquid continuously covered the top of the sand specimen during both the injection and retention periods [5]. During the retention period, the outlet tube was bent upwards to ensure column saturation (Fig. 1b). The tube had an inner diameter of 5 mm, and when the tube was bent upwards, the liquid in the tube was of the same height as the liquid in the soil column. The volume of liquid in the tube was about 5% of the volume of liquid in the soil pores. The amount of chemicals remaining in the outlet tube and above the soil column were not included in the calculation of chemical transform efficiency, since they were not within the soil matrix.

In total, six different MICP treatment protocols (involving different concentrations of cementation solution and retention periods) were applied in the soil column experiments (see Table 2). Table 2 also refers to the protocols of Al Qabany and Soga [4] for comparison. Triplicate samples were prepared and tested for each protocol. Although the concentration of cementation solution varied (see Table 2), the total mass of cementation solution injected in terms of the available reactants was kept constant across tests by applying more injections at lower concentrations, or fewer injections at higher concentrations, each of which was 3.0 M (indicated by the concentration of $CaCl_2$) × sample liquid volume. All of the sand column experiments were conducted at room temperature of about 22 ± 2 °C

2.2.2 Unconfined compression strength (UCS) tests

Since the MICP-treated soil samples are normally rock-like soil specimens and are stronger than soils, and because a UCS test is relatively easier to conduct compared with triaxial testing, UCS tests have been widely used in MICP studies. To compare the results with previously published data, UCS tests were therefore performed in this study. Upon completion of the MICP treatments for the soils in the columns, the specimens were flushed with two pore volumes of deionized water to flush all excess soluble salts prior to removing the specimens from the columns and drying them at 100 °C for at least 24 h before conducing unconfined compression strength (UCS) tests. Since moisture conditions affect the UCS results of tested samples, it is a common practice to oven-dry the MICP-treated soil samples [4, 9, 15, 18, 20, 21, 24, 28, 29]. The top and bottom parts of the samples were trimmed to remove potentially disturbed or uneven zones. The UCS experiments were conducted following the ASTM [1] D2938-86

Table 2 Parameters of macroscale soil column experiments

| Protocol No.	Chemical concentration	Retention time (h)	Normalized input rate (mole/l per h)	References
S1	0.25 M Calcium chloride	6	0.042	[4]
S2		12	0.021	This study
S3		24	0.010	This study
S4	0.50 M Calcium chloride	12	0.042	[4]
S5		24	0.021	This study
S6		48	0.010	This study
S7	1.00 M Calcium chloride	24	0.042	[4]
S8		48	0.021	This study
S9		96	0.010	This study

and ASTM [2] D7012-14e1 standard test method for intact rock core specimens. The axial load was applied at a constant rate of 1.14 mm/min. The length of the sample was measured before UCS tests, and the height-to-diameter ratios were about 2:1, with any deviations being corrected based on Eq. 5 as suggested by the ASTM D2938-86-standard test method [1]:

$$C = \frac{C_a}{0.88 \ + \ (0.24 \ D/H)} \tag{5}$$

where C is the computed compressive strength of an equivalent $H/D = 2$ specimen; C_a is the measured compressive strength; D is the core diameter; and H is its height.

2.2.3 Assessment of CaCO₃ content and chemical efficiency

Calcium carbonate ($CaCO_3$) content and chemical efficiency are generally quantified for MICP-treated samples to evaluate the amount of $CaCO_3$ formed in the soil columns and the percentage mass of calcium ions and urea that transformed to $CaCO_3$. Their comparison enables the development of a better understanding of MICP behaviours aiming to eventually optimize MICP treatment protocols. The $CaCO_3$ content of MICP-treated soil samples was determined using the standard test method for rapid determination of carbonate content of soils [3]. About 20 to 30 g of MICP-treated silicon sand was placed in the reaction chamber and the $CaCO_3$ in the specimen reacted with HCl, generating CO_2 (Eq. 6) which in turn increased the pressure inside a closed chamber. The actual amount of $CaCO_3$ was calculated based on a calibrated relationship (Eq. 7) between the CO_2 pressure and the amount of pure analytical grade $CaCO_3$ powder [2]. $CaCO_3$ content is defined as the calculated mass of $CaCO_3$ divided by the mass of pure sand containing the $CaCO_3$.

$$CaCO_3 + 2HCl \rightarrow CaCl_2 + CO_2 \uparrow + H_2O \tag{6}$$
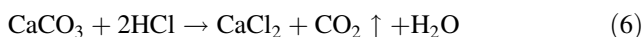
$$CaCO_3 \, mass(g) = pressure \times 1.922 + 0.011. \tag{7}$$

The mass of $CaCO_3$ produced in the soil is affected by the amount of $CaCl_2$ and urea injected into the soils and by the chemical efficiency. Chemical efficiency is defined as the percentage ratio of the measured mass of $CaCO_3$ actually produced, divided by the theoretical mass of $CaCO_3$ which would have been obtained assuming that all the $CaCl_2$ injected into the soil pores is transformed into $CaCO_3$ [5, 25, 27].

2.2.4 Scanning electron microscopy (SEM)

To characterize the shapes, sizes and distribution of precipitated $CaCO_3$ crystals inside the soil specimens, scanning electron microscope (SEM) images of MICP-treated soil samples were captured after the UCS test using a Philips XL20 scanning electron microscope (Philips Electron Optics, Eindhoven, The Netherlands). The tested samples were dried in an oven at 100.5 °C for 24 h. Images were taken at 300 × magnification.

3 Results

3.1 Precipitation process and time-dependent characteristics of crystals when the intervals between injections are short (Protocol M1)

To observe the $CaCO_3$ precipitation process in the short injection interval protocol (Protocol M1), images of a 6 mm by 6 mm square in the middle of the microfluidic chip taken at the ends of the injection intervals between two successive cementation solution injections are shown in Fig. 2a. To analyse the crystal precipitation patterns, a red grid was placed to divide the image into 100 of 0.6 mm by 0.6 mm cells (small squares), as shown in Fig. 2b, d. The 0.6 mm by 0.6 mm squares were valued as 0% when the squares were occupied by dispersed large crystals, as shown in Fig. 2c, whereas the squares were valued as 1% when the squares were mainly occupied by dense small crystals, as shown in Fig. 2e. The crystal precipitation pattern of the 6 mm by 6 mm square was quantified by adding the values of the small squares. The quantification result of Fig. 2a using this method is shown in Fig. 2f. It can be seen from Fig. 2a, f that, after the first injection of cementation solution, the pore space in the microfluidic chip was mainly precipitated by dispersed large crystals. However, after the second injection of cementation solution, dense small crystals started to precipitate and were stable until the completion of the 12th injection of cementation solution.

To observe the precipitation behaviour of $CaCO_3$ crystals in Fig. 2a in detail, one of the middle sections in the microfluidic chip taken at the completion of each cementation solution injection event is shown in Fig. 3. The crystals formed after the first injection were large and remained present after the final injection (indicated by arrows in the first and twelfth images of Fig. 3). In addition, some other large crystals formed after the second injection (indicated by circles in the second and twelfth images of Fig. 3). The small crystals shown after the 12th injection were mainly formed after the second injection of cementation solution. In general, the crystals continued growing once formed during the 12 injections of cementation solution.

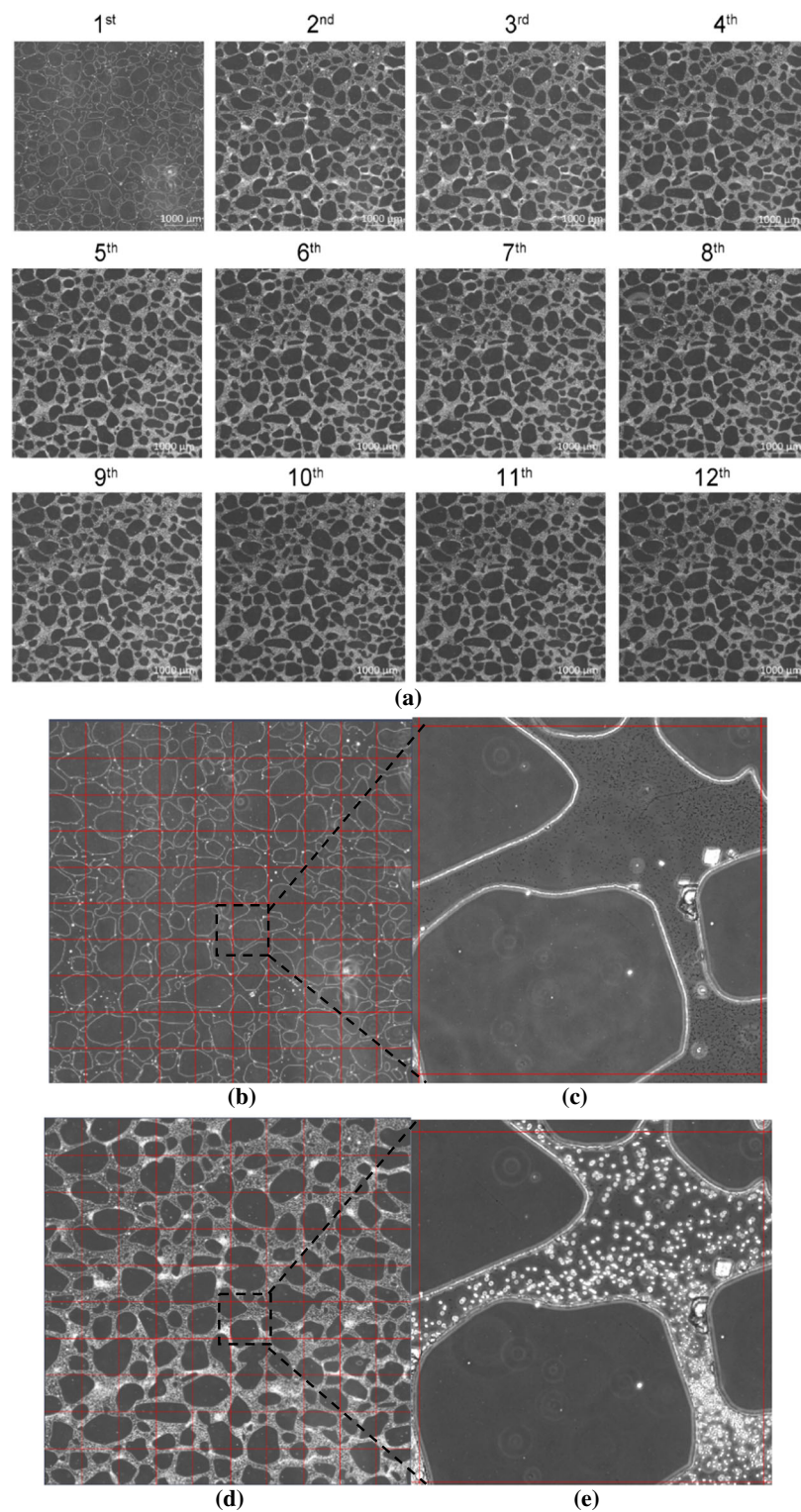To quantify crystal sizes during the treatment procedure of protocol M1 (short injection interval), images of 2 mm

Fig. 2 Crystal growth pattern in the short injection interval case. **a** Microscope images of the centre 6 mm by 6 mm squares taken at the completion of the injection interval of each cementation solution injection; a grid was placed with a cell size of 0.6 by 0.6 mm (**b** and **d**), to analyse the precipitation patterns (c and e). **c** Crystals were mainly small dense crystals, and the square is counted as 100%; **d** crystals were large dispersed crystals, and the square is counted as 0%; **f** area percentage of small crystals plotted against injection numbers

(f)
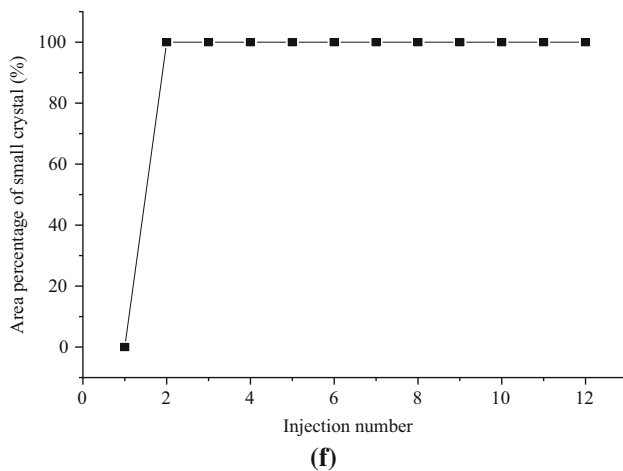
Fig. 2 continued

by 2 mm squares taken at the centre of the microfluidic chip were selected. Images taken at 3 h after the completion of the first and the last injection of cementation solution (Fig. 4a, b, respectively) show that the crystals were mainly large crystals after the first injection (denoted by red circles), whereas after the last injection, there were both large (denoted by red and blue circles) and small crystals (white dots). Since the number of large crystals was relatively small and therefore all of the crystals could be measured, the diameters of crystals shown in the square (Fig. 4a) after each of the injections of cementation solution were measured. However, because the number of small crystals in this area was enormous and it was difficult to measure all of them, twelve 70 μm by 70 μm squares (denoted by blue squares shown in Fig. 4c) in the pores in the central 2 mm by 2 mm area of the microfluidic chip were randomly selected, and the magnified image of one quantified zone is shown in Fig. 4b. The number of small crystals was counted, and the diameters were measured. The total volumes of the crystals relative to the total volume within each of these zones were calculated. The quantification of large and small crystals is shown in Fig. 5.

The box plots of the diameters of large crystals at the completion of the injection intervals after the 1st, 3rd, 5th, 8th and 12th injections are shown in Fig. 5a. The box plots of the diameters of small crystals at the completion of the injection intervals after the 3rd, 4th, 5th, 7th, 8th and 12th injections are shown in Fig. 5b. The mean diameter of the large crystals after the first injection of cementation solution is about 30 μm, and the diameter increases to about 42 μm by the completion of the last injection. The mean diameter of the small crystals after the third injection of cementation solution is about 6.5 μm, and the diameter increases to about 9 μm by the completion of the last injection. The number of large crystals formed after each of

the twelve injections of cementation solution remained almost constant and was about 100 per 1 mm^3. The number of small crystals was about 80–400 crystals per 10^6 $μm^3$, which is equivalent to 8×10^4–4×10^5 per 1 mm^3.

The total volumes of the crystals (V_c) relative to the volumes of the voids (V_v) in the 2 mm by 2 mm calculated zone are plotted against injection number in Fig. 5c. The ratio V_c/V_v for large crystals increases linearly with the increase in injection number, from about 1% after the first injection of the cementation solution to about 2.3% after the last injection. The V_c/V_v for small crystals increases from about 1.5% after the third injection of the cementation solution to about 4.4% after the 7th injection. After subsequent injections, the growth rate of the small crystals starts reducing and the V_c/V_v only increases by about 1.6% using the last five injections (from the 7th to the 12th injection). The V_c/V_v for all large crystals and small crystals increases from about 1% to about 8% over the 12 injections of cementation solution. In the short injection interval experiment, the large numbers of small crystals contribute about two-thirds of the whole precipitation (Fig. 5c). The growth rate of all the crystals gradually reduces from about 1% per injection between the 1st and 3rd injection, to about 0.9% per injection between the 3rd and 5th injection, to about 0.47% per injection between the 5th and 8th injection, and then to about 0.35% per injection between the 8th and 12th injection (Fig. 5c). This is consistent with the reduction in chemical transformation with each subsequent injection (Fig. 5d). The chemical transformation efficiency falls from 100% after the five injections to about 85% after the 8th injection and further reduces to about 69% after the 12th injection (Fig. 5d). The reduction in chemical transformation efficiency as the injection number increases might be due to the reduction in bacterial cell number caused by the injection of cementation solution [32].

3.2 Precipitation process and time-dependent characteristics of crystals when the intervals between injections are long (Protocol M2)

To study the effects of increasing the interval between injections on the precipitation process of MICP, protocol M2 with an injection interval of 24 h was conducted. The precipitation process of the $CaCO_3$ crystals in Protocol M2 is shown in the 6 mm by 6 mm images of the same microfluidic chip taken at the completion of the injection interval after each of the cementation solution injections (shown in Fig. 6a). The quantification of Fig. 6a by the method described in Sect. 3.1 is shown in Fig. 6b. After the first injection of cementation solution, the pore space of the microfluidic chip was mainly filled with dispersed large crystals, but after the second injection of cementation
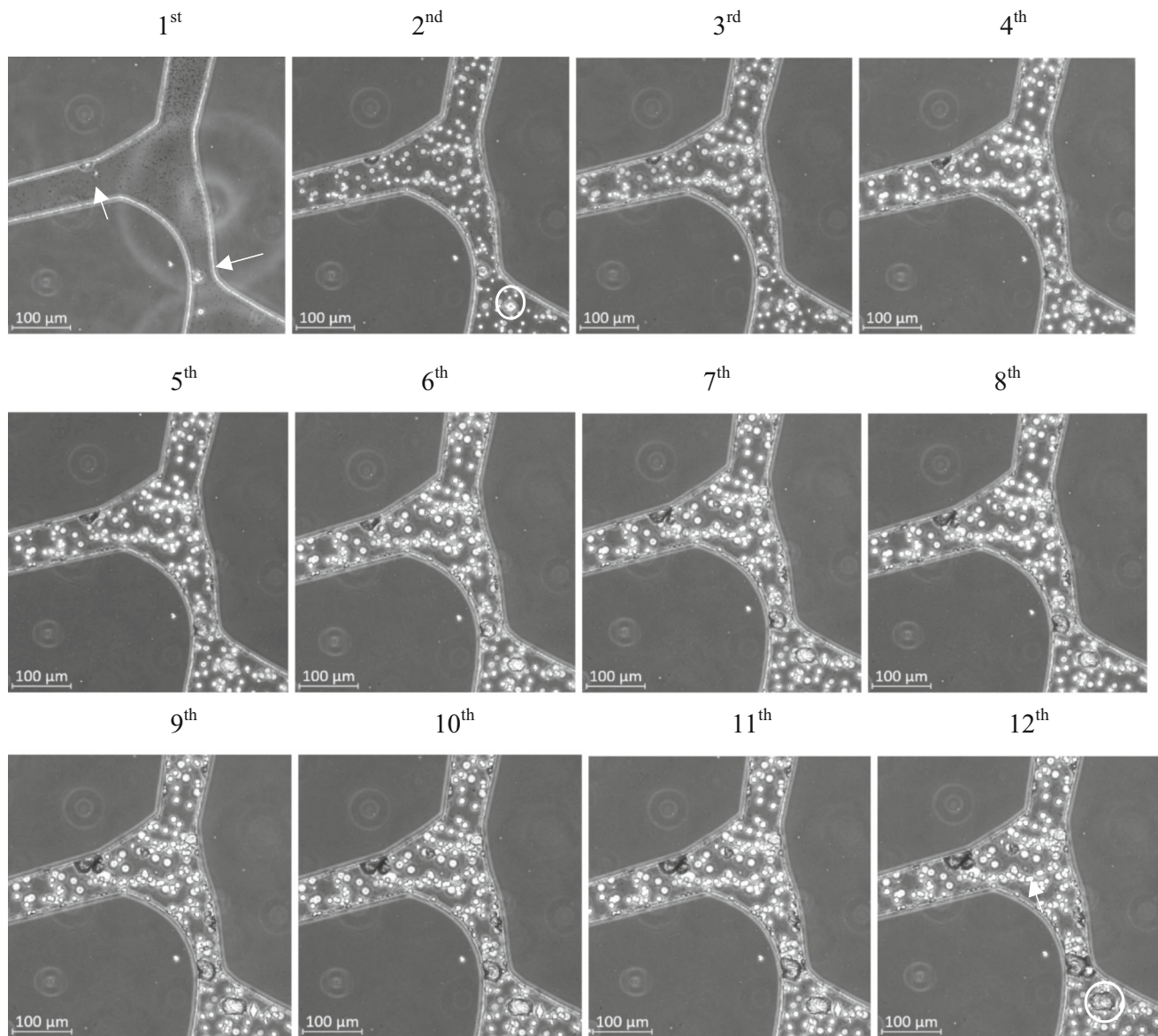
Fig. 3 Images taken at the centre of the 6 by 6 mm square after the completion of the injection interval of each cementation solution injection (short injection interval case)

solution, dense small crystals started to precipitate. The total amount of space occupied by dense small crystals continued increasing until the 3rd injection to about 100%, after which the area occupied by dense small crystals started reducing to about 20% by the 12th injection of cementation solution.

To observe the precipitation behaviour of $CaCO_3$ crystals in Fig. 6a in detail, one of the middle sections in the microfluidic chip taken at the completion of the injection interval between each of the cementation solution injections is shown in Fig. 7. The crystals formed after the first injection were large and remained present after the final injection (indicated by arrows in the 1st and 12th images of Fig. 7). In addition, some other large crystals formed after

the second injection (indicated by circles in the 2nd and 12th images of Fig. 7). The growth behaviour of the small crystals is different compared to the short injection interval case. The dissolution of both small and large crystals can be seen in this case (Fig. 7), which was not observed when short injection intervals were used (Fig. 3).

To quantify the growth rate of the crystals in Protocol M2, the areas from the images which were selected for analysis (Fig. 8a) were the same as the short injection interval case. The large crystals at the completion of the last injection are partially from the ones after the first injection (indicated by red circles in Fig. 8a, b) and partially from the other injections (indicated by blue circles in Fig. 8b). In addition, apart from the fact that small crystals dissolved, some of the large
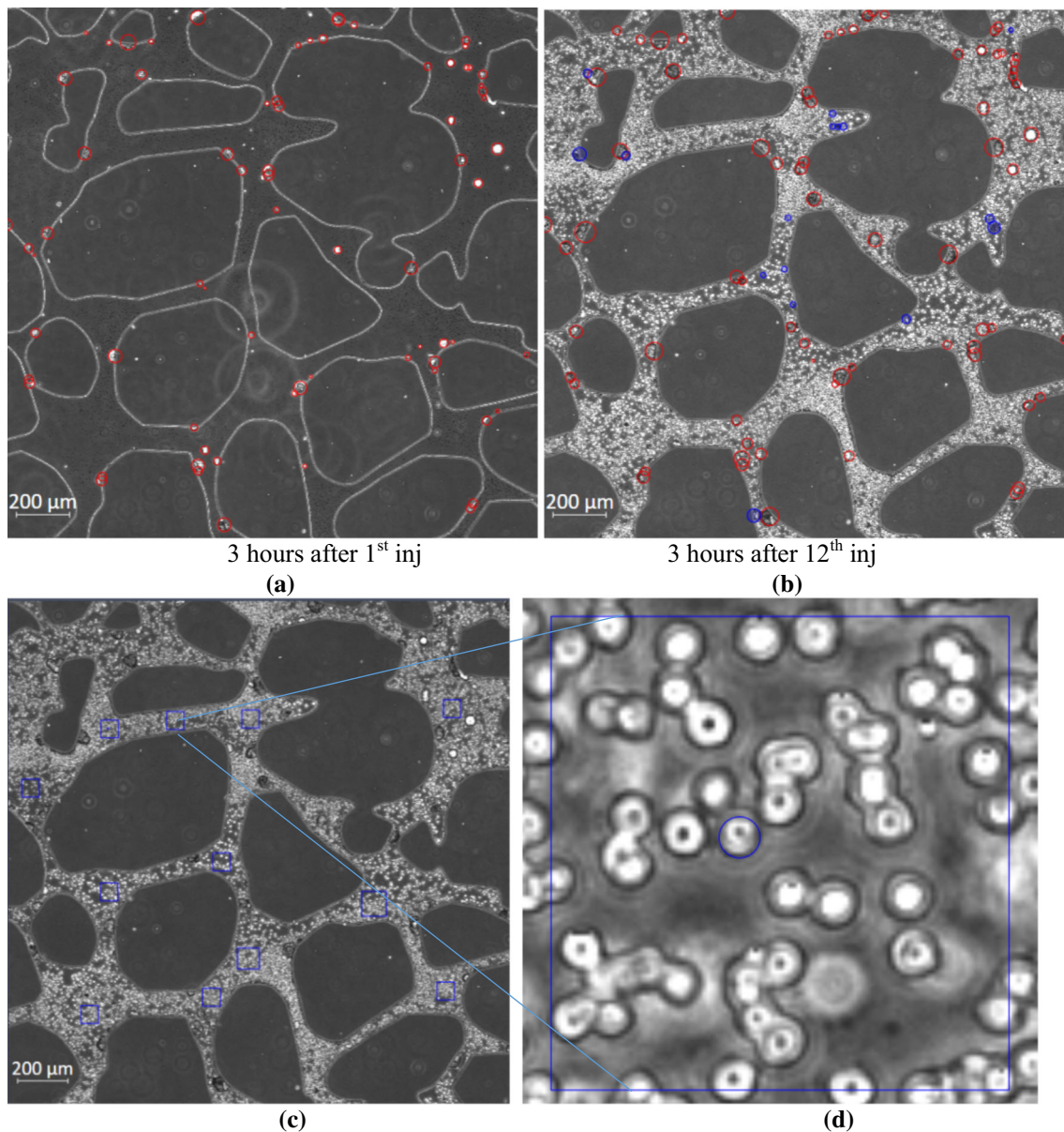
Fig. 4 Microscope images for quantification. **a**, **b** Images taken at the centre of the microfluidic chip at the completion of injection interval after the first and the last injections of cementation solution; **c** image taken at the centre of the microfluidic chip at the completion of injection interval after the last injection of cementation solution, with 12 of 70 μm by 70 μm squares for quantifying small crystal size; **d** magnified image of one of the 70 μm by 70 μm squares shown in Fig. 4c

crystals that precipitated earlier also dissolved after later injections (indicated by purple circles and yellow arrows in Fig. 8c). The proportion of total volume occupied by the dissolved large crystals is about 10%. The box plots of the diameters of large crystals that appeared from the first injection measured at the completion of the injection intervals after the 1st, 3rd, 5th, 8th and 12th injections are shown in Fig. 8d. The mean diameter of the crystals after the first injection of cementation solution is about 30 μm, which is the same as in the short injection case (Fig. 5a). The diameter of crystals increased to about 60 μm by the completion of the

last injection, which is larger than that in the short injection interval case (Fig. 5a). The V_c/V_v values of the total volumes of all large crystals increase linearly from about 0.8% to about 9% over the 12 injections of cementation solution (Fig. 8e). The chemical transformation efficiency indicated by only large crystals remains between about 75% and 85% over the twelve injections (Fig. 8f). The high chemical transformation efficiency calculated by only considering large crystals, which indicates that the majority of crystals in the long injection interval case are large crystals, is different to that for the short injection interval, where small crystals
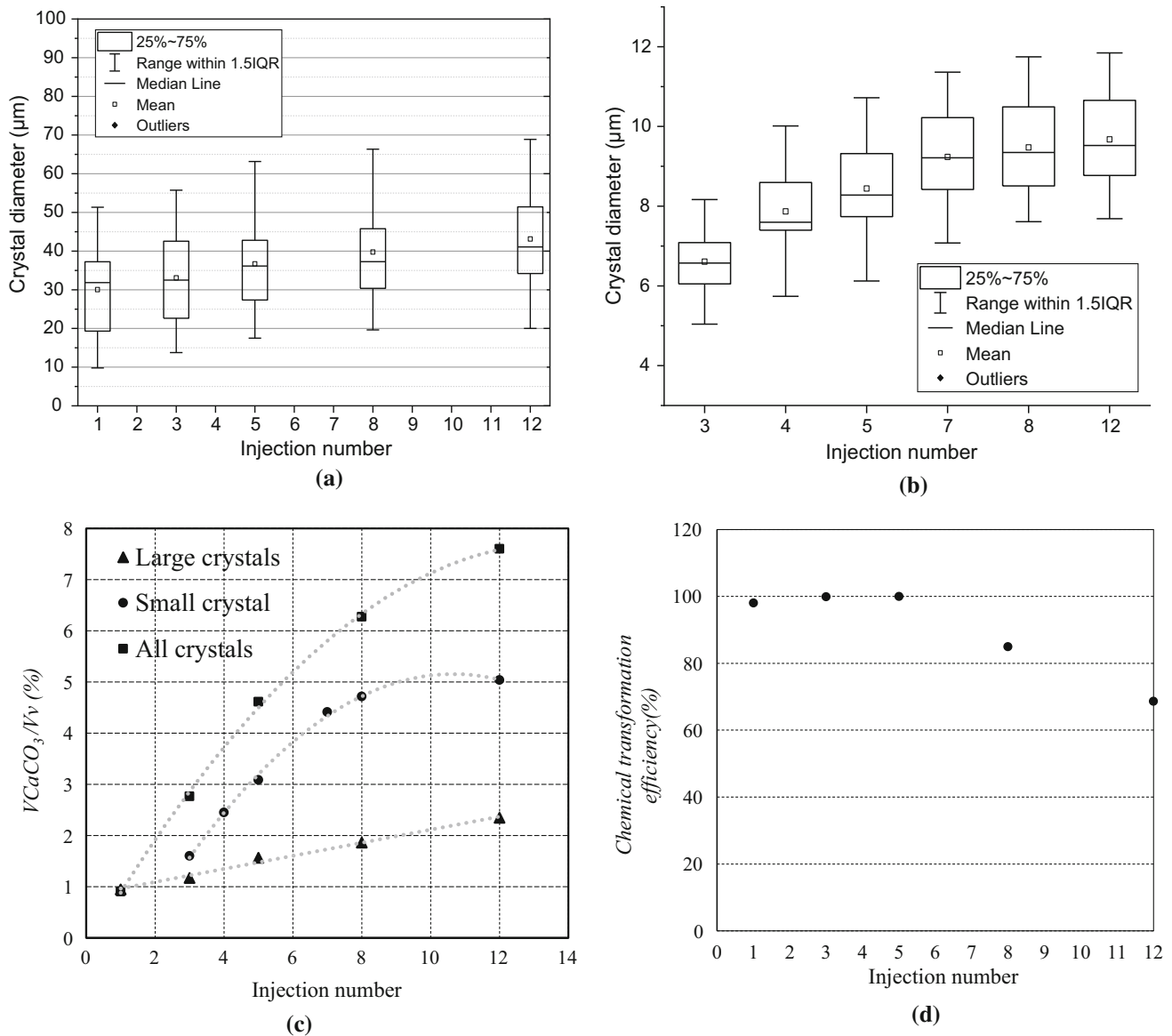
Fig. 5 Quantification of crystals formed in protocol M1. **a** Box chart of the diameters of large crystals at completion of the injection intervals after the 1st, 3rd, 5th, 8th and 12th injections; box chart of 12 crystals, each from the 12 squares in Fig. 4d, at the completion of injection interval after the 3rd, 4th, 5th, 7th, 8th and 12th cementation solution injection; **c** void ratio of large, small and all crystals (Vc) to the corresponding volume of the voids (V_v) in the 2 mm by 2 mm calculated zone plotted with the injection number; **d** chemical transformation efficiencies of all small and large crystals at the completion of injection interval after the 1st, 3rd, 5th, 8th and 12th cementation solution injection of the short injection interval protocol

(crystal sizes smaller than 10 μm) contribute to about two-thirds of the whole precipitation (Fig. 5c). Because the quantification of the small crystals was not conducted in this case, the chemical transformation efficiency would be higher than the reported value, especially after the first few injections when the channels predominantly contained small crystals (Fig. 7). Therefore, the total chemical efficiency which takes all crystals into account should be similar to the one in the short injection case (Fig. 5d), in which the transformation efficiency was higher after the first few injections than after later injections.

3.3 Precipitation–dissolution of CaCO₃ when higher concentrations of cementation solution are used (Protocols M3 and M4)

The concentrations of cementation solution normally used for MICP treatment are between 0.25 and 1.0 M. To investigate whether the precipitation–dissolution–reprecipitation process also occurs when the concentration of cementation solution was 0.5 M or 1.0 M, Protocols M3 and M4 were conducted. A long injection interval of 24 h was used between each injection. Microscope images of
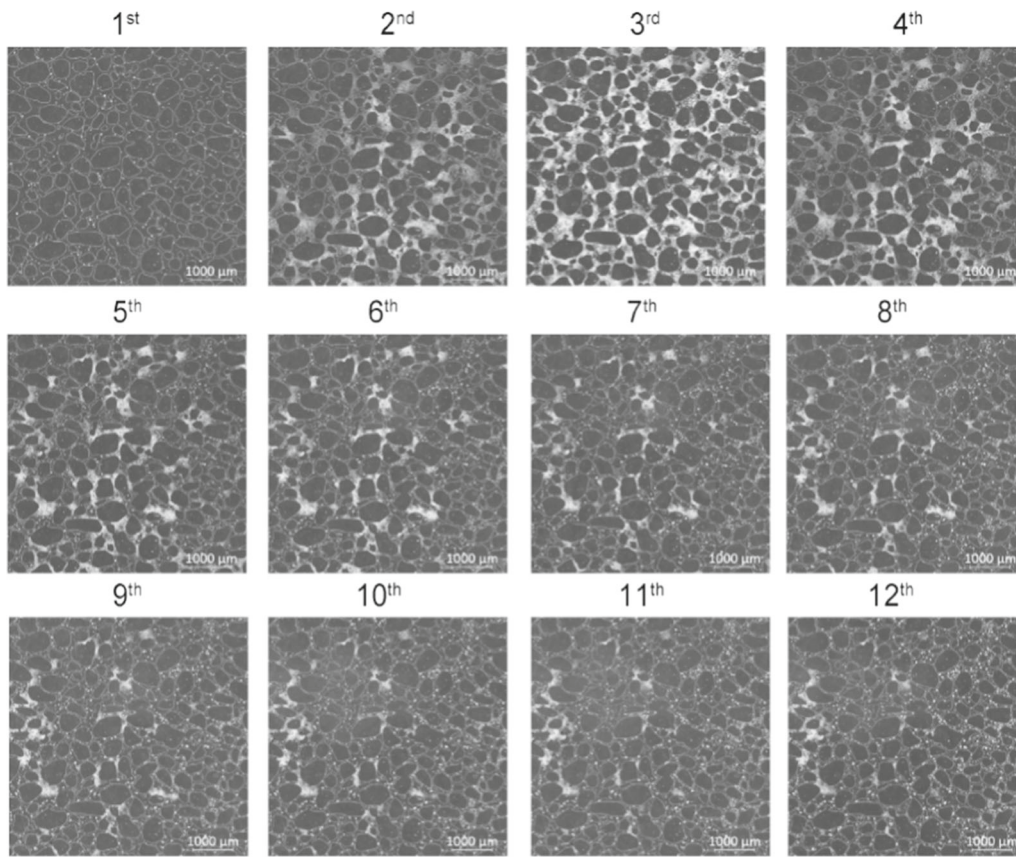
(a)
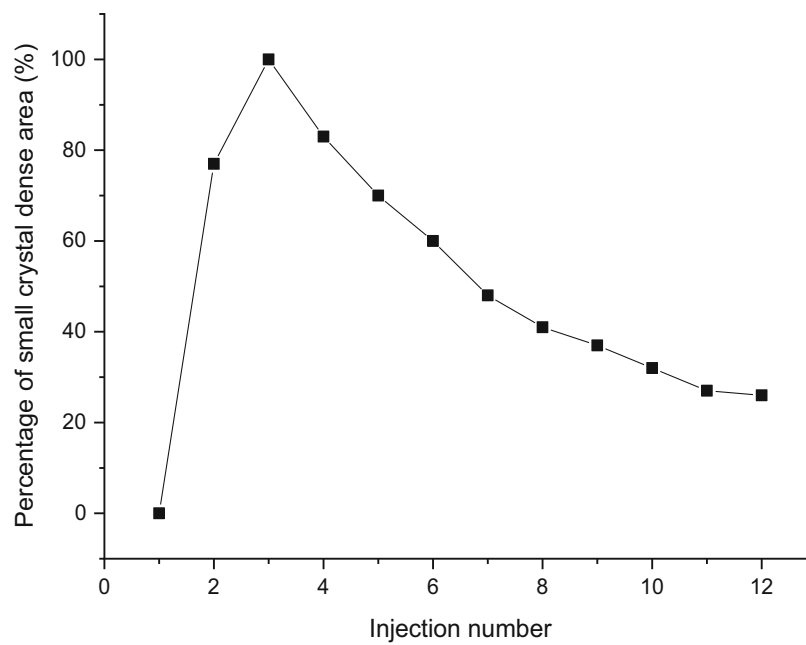
(b)

Fig. 6 **a** Microscope images of microfluidic chip (Protocol M2—the long injection protocol) at the completion of the injection interval of the 12 injections of cementation solution; **b** area percentage of small crystals plotted against injection numbers
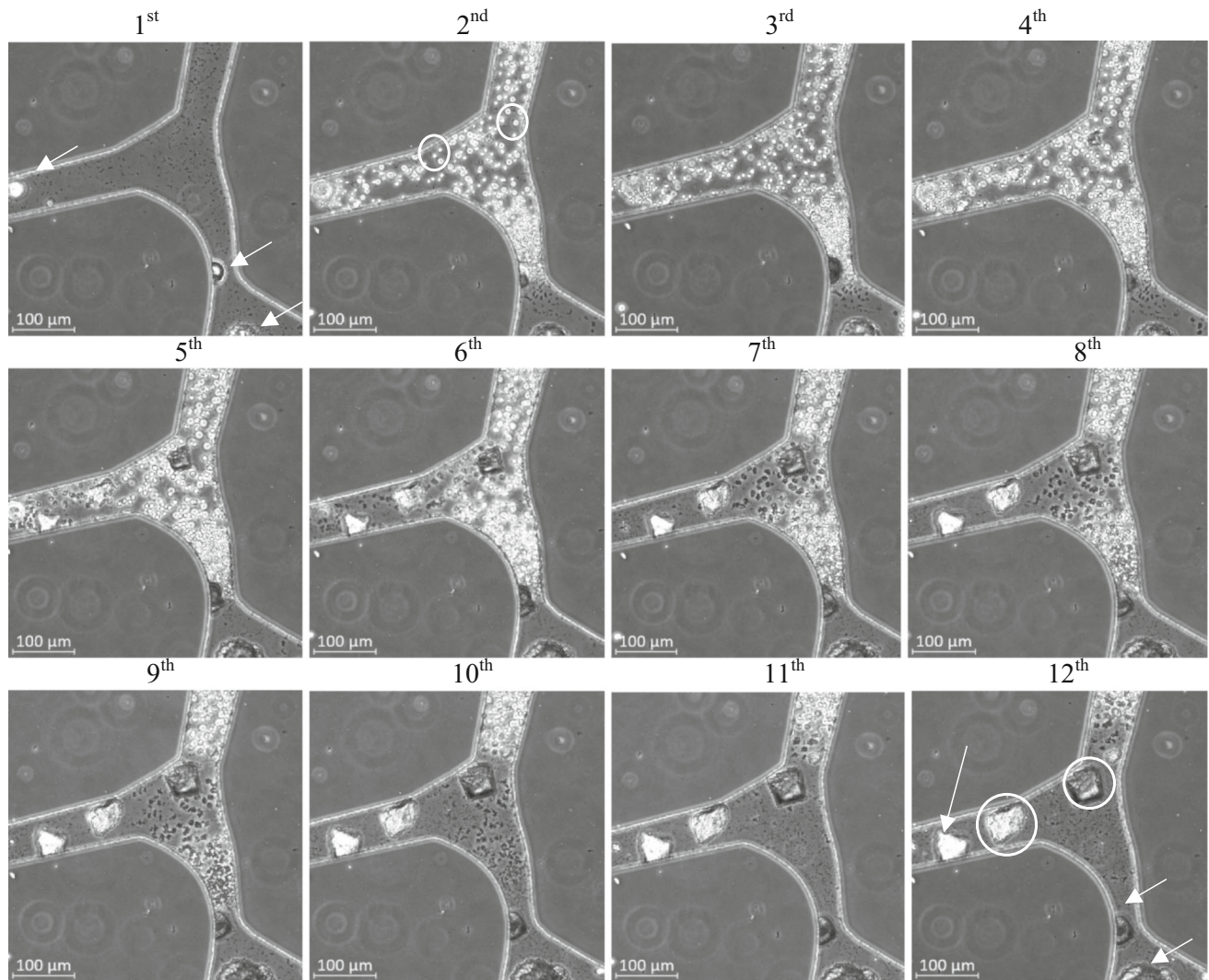
Fig. 7 Images of a cell located at the centre of the 6 by 6 mm square taken after the completion of the injection interval of each cementation solution injection (long injection interval case)

250 µm × 250 µm squares at 1, 3, 6 and 24 h after the completion of the first and second injection of cementation solution for the 0.5 M and 1.0 M case are shown in Fig. 9a, b, respectively. Similar to what was observed in the 0.25 M case, small crystals were also formed after the second injection of cementation solution, subsequently dissolved and were replaced by larger crystals.

3.4 Correlations between unconfined compressive strength (UCS) and CaCO₃ content in MICP-treated sands

To investigate whether the observations made from microfluidic chip experiments can be used to optimize MICP treatment protocols for soil strength enhancement, soil column experiments and UCS tests were conducted. All samples failed with a tensile-like failure in unconfined

conditions, similar to the results reported in previous research [5, 31] and Cheng et al. 2012). Correlations between the $CaCO_3$ content and UCS were normally derived to study the effect of $CaCO_3$ content on the strength of MICP-treated soils [4, 9, 15, 20, 24, 28, 29, 31]. The correlations between the $CaCO_3$ content and UCS of this study and Al Qabany and Soga [4] are shown in Fig. 10c.

For example, Fig. 10 shows that the UCS varies from 1.8 to 5.6 MPa at the same $CaCO_3$ content of 7%. These large variations in strength at the same cementation level are consistent with the results reported by Wang et al. [34] because the $CaCO_3$ crystals have different characteristics depending on the MICP treatment protocols. In addition, when the concentration of cementation solution is the same, higher UCS values were obtained when the injection interval was longer. For example, when the concentration
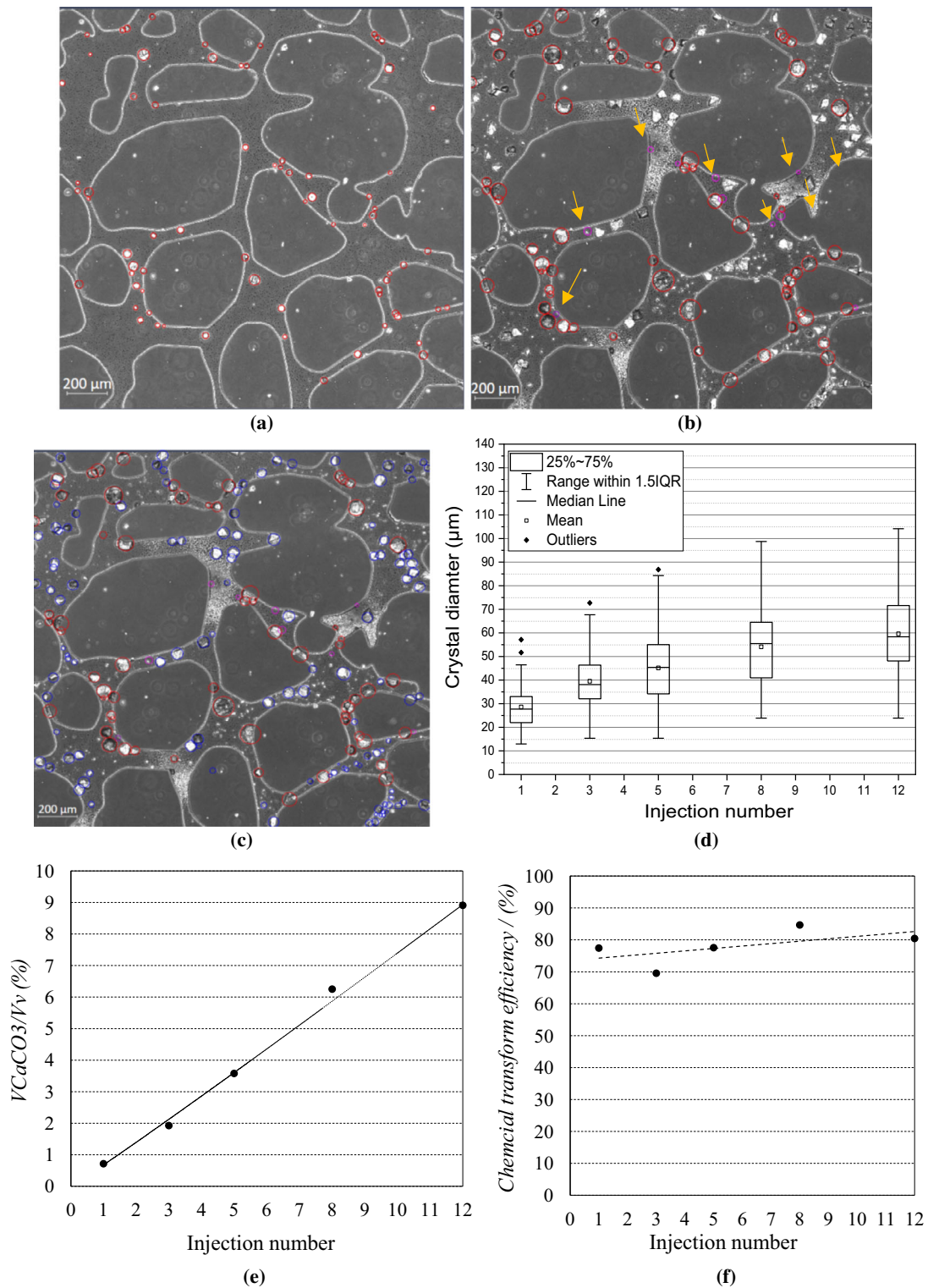
Fig. 8 Quantification of large crystals in the long injection protocol case. **a-b** Images at the centre of the microfluidic chip taken at the completion of injection interval after the first and the last injections of cementation solution. **c** Images at the centre of the microfluidic chip taken at the completion of injection interval after the last injections of cementation solution indicating that the crystals started growing after the completion of the first injection; **d** box plots of the diameters of large crystals at completion of the injection intervals after the 1st, 3rd, 5th, 8th and 12th injections. **e** void ratio of large, small and all crystals (Vc) to the corresponding volume of the voids (V_v) in the 2 mm by 2 mm calculated zone after the 1st, 3rd, 5th, 8th and 12th injections; **f** the chemical transformation efficiency calculated by the total volume of only large crystals
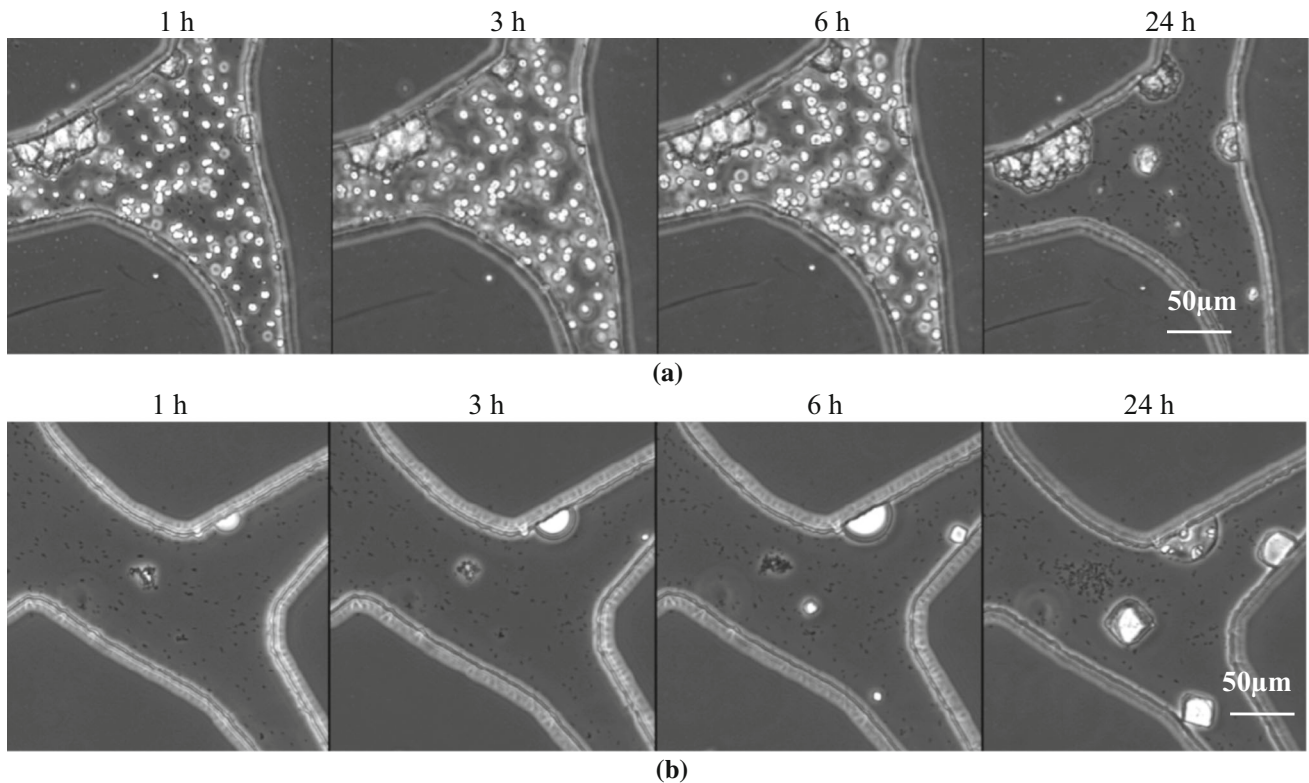
Fig. 9 Microscope images of 250 μm by 250 μm square at one pore of microfluidic chips at 1, 3, 6 and 24 h after the completion of the second injection of cementation solution (0.5 M) and first injection of cementation solution (1.0 M)

is 0.5 M, the 48-h injection interval (denoted by solid round dots) results in UCS values between about 3 Mpa and 5.5 Mpa at a CaCO$_3$ content between 6.4% and 7.4%, whereas the 12-h injection interval (denoted by hollow round dots) results in UCS values of only 0.4 Mpa to 1.2 Mpa at a similar CaCO$_3$ content. Furthermore, the UCS values of samples treated with 1.0 M cementation solution are in general lower than the UCS values of samples treated with cementation solution of 0.25 M or 0.5 M when the injection interval is the same. The low UCS values at 1.0 M are mainly due to the inhomogeneity of samples [4].

To compare the efficiency of CaCO$_3$ in increasing the strength of soils, normalized UCS values were obtained by dividing the UCS values by the CaCO$_3$ content of each of the dots in Fig. 10 (results shown in Fig. 11). The data obtained for the 9 protocols (shown in Table 2) are shown in the 9 columns. At all chemical concentrations, reducing the normalized input rate resulted in an increase in the efficiency with which CaCO$_3$ enhanced the strength of the specimens (shown when comparing the three columns in each chemical condition). The normalized UCS values per 1% of CaCO$_3$ samples treated over a 6-day period using 0.25 M, 0.5 M and 1.0 M cementation solution were 3.6.-, 4.9- and 3.9-fold higher than those treated over a period of 3 days, respectively. UCS values increased further by 1.22-, 1.27- and 1.33-fold, respectively, when the total treatment

duration increased from 6 to 12 days. In addition, the higher the chemical concentration was, the lower the efficiency of CaCO$_3$ in increasing the strength of soils was (shown when comparing the three columns of the same normalized input rate cases). This is consistent with the conclusion obtained by Al Qabany and Soga [4] that performing more injections of lower concentrations of cementation solution is better for enhancing soil strength.

3.5 Chemical efficiency of cementation solution transforming into cement in the soil column experiment

The chemical efficiencies quantified in the soil column treated by protocols S2, S3, S5, S6, S8 and S9 (Table 2) are shown in Fig. 12. When the concentration of cementation solution was either 0.25 M or 0.5 M, the chemical efficiency was relatively high (higher than 75%). These results are consistent with the microfluidic chip experiment, as well as with the studies conducted by Al Qabany et al. [5], 10 and Konstantinou et al. [19]. In contrast, when the concentration of cementation solution was 1.0 M, the mean chemical efficiency was lower (71% for a 48-h injection interval treatment and 64% for a 48-h injection interval treatment), since the long injection intervals likely caused a decrease in bacterial activity due to the higher molarity
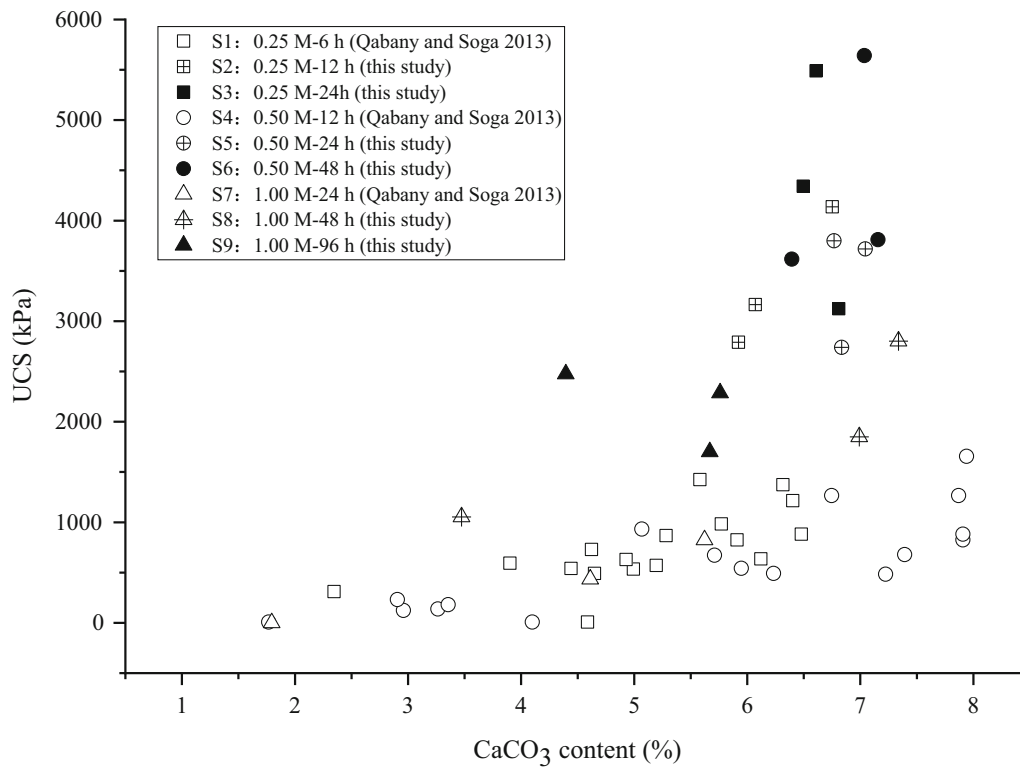
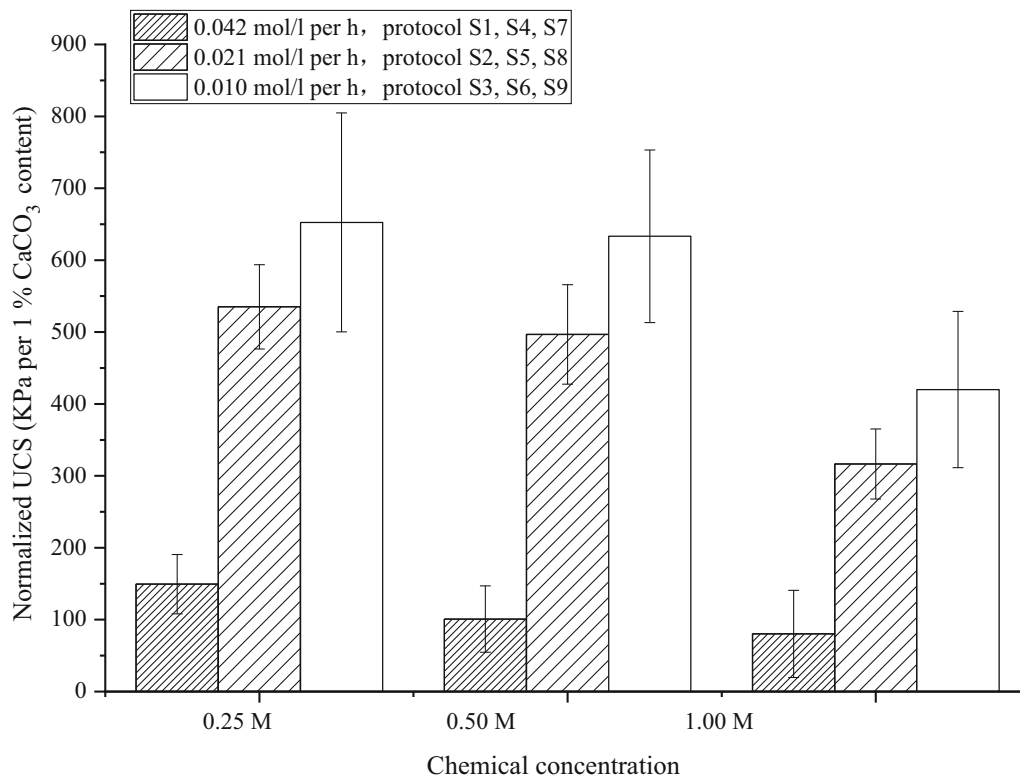**Figure10** CaCO$_3$ content vs UCS (comparison with the results of [4])

Fig. 11 UCS values normalized by CaCO$_3$ content

entombing some of the bacteria over time. However, the bacterial activity inside the soil is difficult to measure. In addition, the variation in chemical efficiency between samples treated with the same MICP procedure, shown by the error bars in Fig. 11, was large when the cementation solution concentration was 1.0 M. The large variations in efficiencies indicate the inhomogeneity of soil samples, which is consistent with the results obtained by Al Qabany et al. [5].

3.6 Microscale properties of CaCO₃ crystals obtained in the soil column experiment

To observe the CaCO₃ crystals after the MICP treatment of the macroscale specimens, scanning electron microscope (SEM) images were taken (see Fig. 13). When the concentration of cementation solution is the same, the crystals in the samples treated with longer retention periods are larger than those with shorter retention periods. For example, when the concentration of cementation solution was 0.25 M, the average size of the crystals increased from about 5 μm when a 6-h injection interval was used, to about 40 μm when the interval between injections was 12 h and to about 60 μm when the injection interval was 24 h. The pattern of changes in crystal size in relation to the change in injection interval is in agreement with the results obtained in the microscale experiments (Fig. 13 compared to Fig. 3 and Fig. 7).

4 Discussion

4.1 Effects of injection interval and concentration of cementation solution on the precipitation processes and characteristics of CaCO₃ crystals

Wang et al. [33] found that precipitation–dissolution and reprecipitation of CaCO₃ occurred after a sample of *S. pasteurii* bacterial suspension was mixed with cementation solution, and used this observation to predict and detect the size of calcium carbonate crystals after MICP treatment by using microfluidic chips. To this end, the present study further explores the differences in the precipitation process and time-dependent characteristics of CaCO₃ crystals in the cases when long or short injection intervals, as well as higher cementation solution concentrations (0.5 M and 1.0 M), were used. When a short injection interval (0.25 M cementation solution with a short injection interval of 3–5 h) was used, large crystals began to precipitate from the first injection onwards, and small crystals began to precipitate from the second injection onwards (Figs. 2, 3). Both large and small crystals remained stable throughout
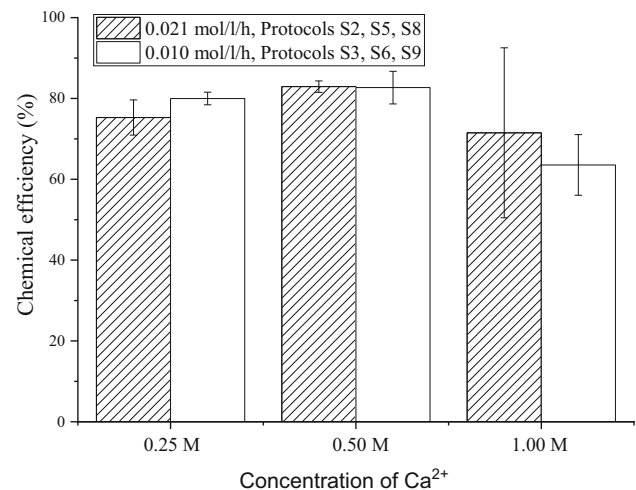
Fig. 12 Chemical efficiencies of the MICP-treated sand samples. Data presented as mean ± standard error, $n = 3$ (n is the number of times each treatment condition and the relative measurement was repeated)

the whole treatment period (Figs. 2, 3). In the case of a long injection interval (0.25 M cementation solution, 24-h injection interval), large crystals also precipitated from the first injection onwards and small crystals precipitated from the second injection onwards, but 10% of large crystals and most of the small crystals dissolved (Figs. 6, 7). The dissolution of small or part of the large crystals contributed to the precipitation of larger CaCO₃ crystals (Fig. 7 compared to Fig. 3). When a higher cementation solution concentration together with a long injection interval was used (0.5 M or 1.0 M cementation solution, 24-h injection interval), more stable crystals grew in size at the expense of the dissolution of less stable crystals during MICP processes (Fig. 9). This process of CaCO₃ precipitation–dissolution–reprecipitation when the injection interval is long, regardless of whether the concentration of cementation solution is 0.25 M, 0.5 M or 1.0 M, is consistent with Ostwald ripening, which is a spontaneous process driven by chemical potential differences among different-sized particles; specifically, larger crystals grow at the expense of smaller ones, with the latter having a higher solubility than large crystals [31, 32, 43, 35].

Due to the difference in precipitation process, the average crystal sizes when short or long injection intervals were used were about 40 μm and 60 μm, respectively (Figs. 5a, 8d). 8×10^4–4×10^5 small crystals per 1 mm³ (sizes smaller than 12 μm by the end of treatment, Fig. 5b) in the short injection interval case contributed to about 66% of the whole precipitation (Fig. 5c), whereas 100 large crystal crystals per 1 mm³ contributed to about 80% chemical transformation efficiency (Fig. 8f). The chemical transformation efficiency during the staged-injection MICP treatment procedure decreased as the number of
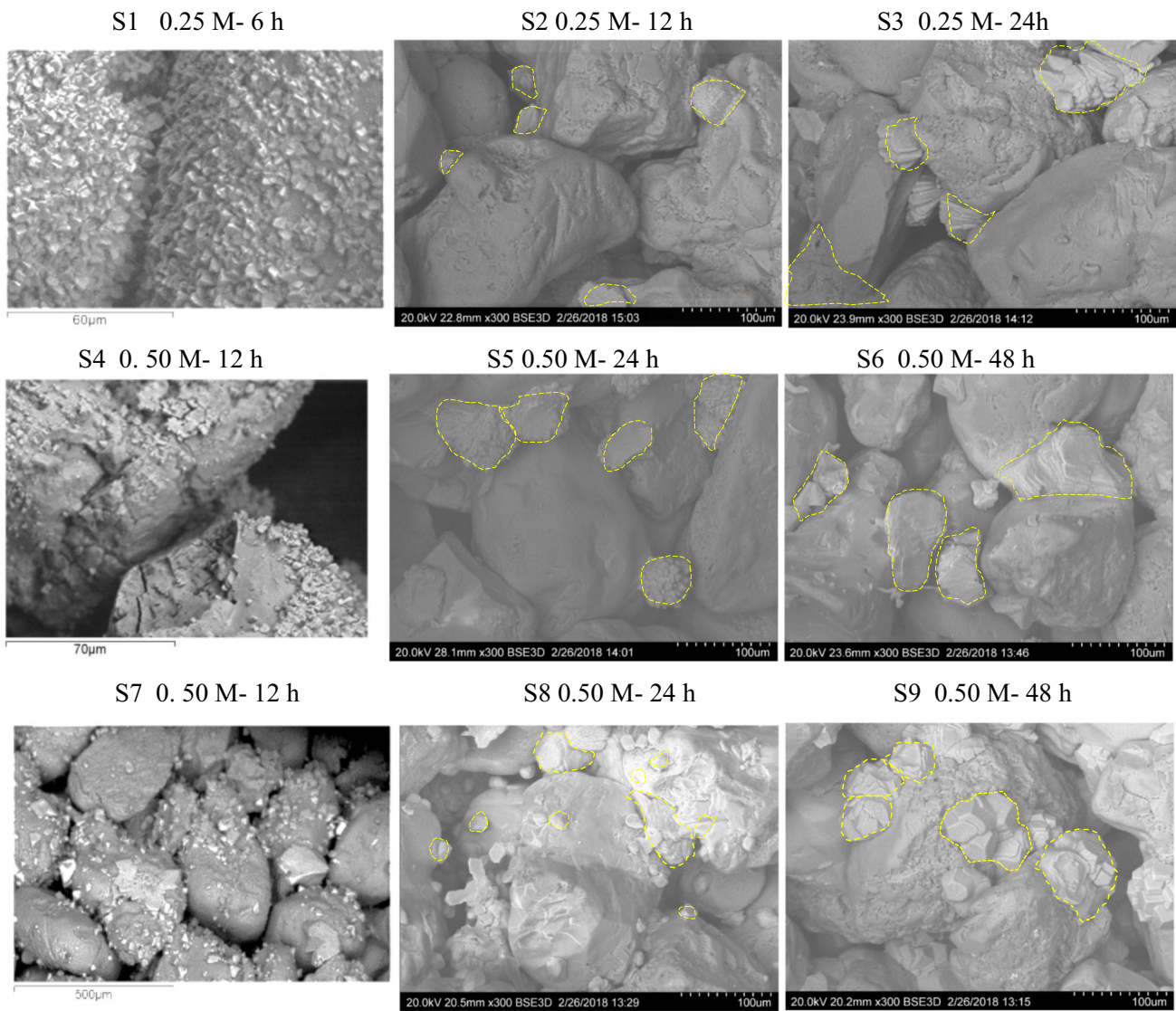
S1 0.25 M- 6 h　　　　　　S2 0.25 M- 12 h　　　　　　S3 0.25 M- 24h

S4 0. 50 M- 12 h　　　　　　S5 0.50 M- 24 h　　　　　　S6 0.50 M- 48 h

S7 0. 50 M- 12 h　　　　　　S8 0.50 M- 24 h　　　　　　S9 0.50 M- 48 h

Fig. 13 SEM images of CaCO$_3$ crystals inside MICP-treated sand samples after MICP treatments. **a** S1, 0.25 M–6 h injection interval treatment, CaCO$_3$ content is 4.8% [5], **b** S2, 0.25 M–12 h injection interval treatment, CaCO$_3$ content is 6.1%; **c** S3, 0.25 M 24-h injection interval treatment, CaCO$_3$ content is 6.6%; **d** S4, 0.25 M 12-h injection interval treatment, CaCO$_3$ content is 6.0% [5], **e** S5, 0.50 M 24-h injection interval treatment, CaCO$_3$ content is 7.0%; **f** S6, 0.50 M 48-h injection interval treatment, CaCO$_3$ content is 7.0%; **g** S7, 1.00 M 24-h injection interval treatment, CaCO$_3$ content is 3.9% [5], **h** S8, 1.00 M 48-h injection interval treatment, CaCO$_3$ content is 7.0%; **i** S9, 1.00 M 96-h injection interval treatment, CaCO$_3$ content is 5.8%

cementation solution injections increased (Fig. 5d), possibly because bacterial activity was reduced due to the removal of bacterial cells from the porous medium by the injections of cementation solution. In addition, increasing the injection interval from 3–5 h to 24 h resulted in an increase in chemical transformation efficiency from 70% to more than 80% by the end of MICP treatment (Fig. 5d compared to Fig. 8f). In the staged-injection procedure, the biochemical reactions started after the injection of cementation solution into the soil matrix. If the next batch of cementation solution is injected before the previous batch of cementation solution finished transforming into

CaCO$_3$, the chemical transformation efficiency of MICP will be low. Al Qabany et al. [5] conducted a series of soil column experiments to determine the optimal injection interval by varying the injection interval and measuring the CaCO$_3$ content at the end of MICP treatment to compare the associated chemical transformation efficiencies. In their study, when the bacterial optical density (OD$_{600}$) was between 0.8 and 1.2, the chemical efficiency remained higher than 80% provided that the cementation solution injection rate was below a threshold of 0.042 mol/l per hour. By contrast, the chemical efficiency decreased when the injection rate exceeded this threshold. 0.042 mol/l per

hour is equivalent to 6-h retention time for the case when the concentration of cementation solution was 0.25 M. The chemical efficiency results observed in the current study are consistent with the results presented in Al Qabany et al. [5].

4.2 Use of microfluidic chips to optimize MICP protocols for strength enhancement

Studies have found that both $CaCO_3$ content and the properties of $CaCO_3$ crystals affect the strength of MICP-treated soils. Soil column experiments, together with UCS testing, triaxial testing and SEM imaging, are the main methods that have been used so far to optimize treatment protocols for enhancing the strength of MICP-treated soils. However, although MICP optimization using soil column experiments and SEM imaging is important, it is also time-consuming. In contrast to soil column experiments, microfluidic chip experiments provide a functional way to observe the MICP precipitation process directly during each of the injections of cementation solution [32, 33]. The time needed for cementation solution to complete transforming into $CaCO_3$ crystals can be directly determined by determining the time point when the crystals stop growing [31]. In addition, changes in $CaCO_3$ morphology and the interactions between bacteria and $CaCO_3$ can also be studied.

In this study, by applying the observations made during microfluidic chip experiments, soils treated using long injection intervals (lower normalized rate of injection) had higher UCS values in samples containing similar amounts of $CaCO_3$ (Fig. 10). In addition, the normalized UCS values of $CaCO_3$ content were higher when the injection intervals were longer, regardless of the concentration of cementation solution (Fig. 11). The higher normalized UCS values obtained after longer injection intervals suggest that a longer injection interval produced $CaCO_3$ crystals that are more efficient in enhancing soil strength. SEM imaging revealed that crystal sizes were larger when the injection interval was longer compared to crystal sizes that were produced when a short injection interval was used (Fig. 12).

Studies have found that crystals which are large enough to fill the gaps between soil particles can prevent particle rotations during shearing, thereby providing more resistance to dilation, which results in increased soil strength [43]. This can explain the reason why a longer injection interval is helpful for strength enhancement (Fig. 12). In addition, this study has also shown that when the crystals are small and large in number, the crystals precipitate over a large area of the soil surface and form a so-called coating precipitation pattern (Fig. 13 a and d). By contrast, when the crystals are large in size and small in number, the

crystals either grow on the parts of the surface where they are adjacent to other soil particles, or on parts of the soil surface that face towards the soil pores, thereby forming a bonding pattern or filling pattern, respectively. The crystals can also form a mixture of two or three of these patterns. For example, during the 2nd to the 8th injections in Fig. 7, crystals formed coating, pore filling and bonding patterns, whilst in Fig. 13g, h, crystals formed a mixture of coating and pore filling patterns.

In microfluidic chips, $CaCO_3$ crystals grow from the top and bottom surfaces of the channels, as well as from the sides of pillars (see Figs. 3, 7, 9), whereas in three-dimensional soil matrices, crystals grow on the surfaces of soil particles. Despite the differences in pore structures between microfluidic chips and real sandy soil matrices, the changes in crystal size and the general crystal distribution (coating, filling and bonding, schematic in Fig. 14) shown in the microfluidic chip experiments are the same as shown in the soil column experiment. Therefore, the microfluidic chip experiment can help to predict the distribution pattern of $CaCO_3$ crystals. These results indicate that the observation made from microfluidic chip experiments helps to enhance the understanding of microscale processes, mechanisms and characteristics of MICP, which can be applied in real sandy soil for MICP strength enhancement.

5 Implications for engineering applications

This study illustrates that increasing injection interval (reducing normalized input rate of cementation solution) increases the average size of $CaCO_3$ crystals, which are more efficient in bonding soil particles, thereby enhancing soil strength. In addition, this research also shows that more injections of lower concentrations of cementation solution tend to enhance soil strength more effectively. However, for practical reasons, the treatment duration and number of MICP injections should preferably be minimized. A balance between optimum soil strength enhancement and the time window of MICP treatment should be considered for MICP engineering applications. The mechanisms which enable the formation of a higher percentage of $CaCO_3$ crystals which bond soil particles within a short treatment time and simpler treatment procedure may also be worth exploring in the future.

In order for MICP to be used for real engineering projects, the effects of local environmental factors such as soil properties, ion content, temperature, oxygen content and local bacterial communities on the behaviour of bacteria, $CaCO_3$ precipitation processes and kinetics, as well as $CaCO_3$ content and microscale characteristics which affect the engineering performance of MICP-treated soils, need to be evaluated beforehand. These effects can be evaluated by
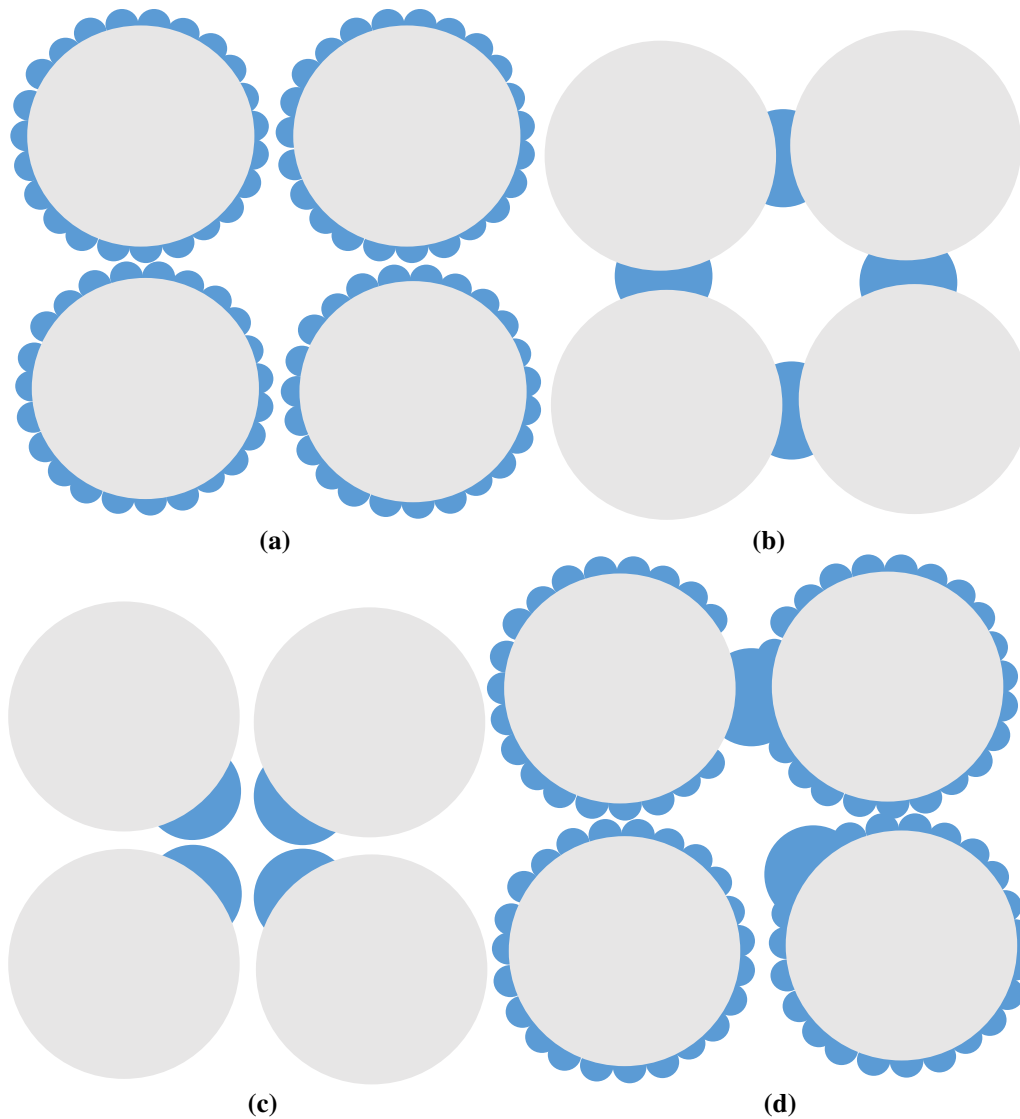
Fig. 14 Schematic of CaCO$_3$ crystal precipitation pattern. **a** Surface coating, **b** bonding, **c** pore filling, **d** mixtured pattern

performing the microfluidic chip experiments, and understanding these effects will be helpful for improving MICP treatment protocols. Combining microfluidic chip experiments with soil column experiments is a useful way to optimize MICP treatment protocols, especially in terms of enhancing soil strength.

Achieving uniformity of CaCO$_3$ content distribution in soil matrices remains challenging for engineering applications. CaCO$_3$ distribution is highly dependent on the reactive transport processes of MICP. So far, several numerical models have been proposed for predicting CaCO$_3$ content, but mostly only for laboratory-scale soil matrices without considering the complex effects of environmental factors on MICP. Inhomogeneous samples have been observed even for core-scale homogeneously produced sandy samples when the concentration of cementation solution was 1.0 M. For engineering applications,

environmental factors and soil inhomogeneity may affect bacterial and chemical transport, bacterial activity and cementation kinetics, thereby making the distribution of CaCO$_3$ crystals more difficult to predict. Combining microfluidic chip experiments with longer column experiments or three-dimensional soil model experiments to investigate the effects of various environmental factors and treatment protocols on the homogeneity of MICP-treated soils may provide a useful way to address this challenge, which still needs to be further explored in future.

6 Conclusions

This study demonstrates an example of using a combination of microfluidic chip experiments and soil column experiments for optimizing soil strength enhancement

protocols. The effects of injection interval and concentration of cementation solution on the properties of calcium carbonate crystals were examined at both the micro- and the macroscale.

Both the microscale microfluidic chip experiments and macroscale column tests indicated that, when the injection interval was shorter (i.e. 3–5 h compared to 24 h for a 0.25 M cementation solution), the resulting crystals were larger in number and smaller in size. In addition, the microscale microfluidic chip experiments showed that large crystals grew at the expense of the dissolution of smaller crystals, regardless of whether the concentration of cementation solution was 0.25 M, 0.5 M or 1.0 M. This could be attributed to Ostwald ripening, a spontaneous process driven by chemical potential differences between different-sized particles, where larger crystals grow at the expense of smaller ones which have a higher solubility than the large ones.

The difference in crystal sizes and numbers substantially affected the strength of MICP-treated specimens. Regardless of the concentration of cementation, reducing the normalized input rate of cementation solution from 0.042 mol/l/h (treated over 3 days) to 0.021 mol/l/h (treated over 6 days) significantly increases UCS values of samples, whereas a further reduction in the normalized input rate of cementation solution from 0.021 mol/l/h (treated over 6 days) to 0.010 mol/l/h (treated over 12 days) slightly increases UCS values of samples. The normalized UCS values per 1% $CaCO_3$ using 0.25 M, 0.5 M and 1.0 M cementation solution were 4.3-, 5.8- and 3.2-fold higher than those treated over a period of 3 days, respectively. The normalized UCS values per 1% $CaCO_3$ of samples treated over a 6-day period using 0.25 M, 0.5 M and 1.0 M cementation solution were 3.6.-, 4.9- and 3.9-fold higher than those treated over a period of 3 days, respectively. UCS values increased by a further 1.22-, 1.27- and 1.33-fold, respectively, when the total treatment duration increased from 6 to 12 days. The less pronounced increase in the strength of soils treated over 12 days compared to 6 days was largely because over a 6-day treatment, the crystals were already relatively large enough to bond the soil particles efficiently and further crystal growth increased soil strength but to a lesser extent.

This study shows that increasing the injection interval and introducing more injections of lower concentration of cementation solution tends to enhance soil strength more effectively. However, for practical reasons, the treatment duration and injection numbers of MICP may preferably be minimized. The mechanisms of forming higher percentage of $CaCO_3$ crystals which bond soil particles within a short treatment of time and simpler treatment procedure may also be worth exploring in future.

The microfluidic chip experiments presented in this research illustrate changes in crystal sizes and numbers with time and provide direct information about the MICP process. This study establishes a link between the results of MICP microscale microfluidic chip experiments and the macroscale column experiments, thereby demonstrating that monitoring microscopic process in microfluidic chip experiments can be useful for optimizing MICP treatment to produce calcium carbonate crystals with desired properties for field applications.

References

1. ASTM (1986) D2938:390-391: Standard test method of unconfined compressive strength of intact rock core specimens. In: 1995 Annual Book of ASTM standards. ASTM, West Conshohocken, PA, USA.
2. ASTM (2004) D7012-14e1: Compressive strength and elastic moduli of intact rock core specimens under varying states of stress and temperatures. ASTM, West Conshohocken, PA, USA.
3. ASTM (2014) D4373–14: Standard test method for rapid determination of carbonate content of soils. ASTM, West Conshohocken, PA, USA.
4. Al Qabany A, Soga K (2013) Effect of chemical treatment used in MICP on engineering properties of cemented soils. Géotechnique 63(4):331–339
5. Al Qabany A, Soga K, Santamarina C (2012) Factors affecting efficiency of microbially induced calcite precipitation. J Geotech Geoenviron Eng 138(8):992–1001
6. Chen, Y., Gao, Y., Ng, C. W. W., & Guo, H. (2021). Bio-improved hydraulic properties of sand treated by soybean urease induced carbonate precipitation and its application Part 1: Water retention ability. Transp Geotech, 27(September 2020), 100489. https://doi.org/10.1016/j.trgeo.2020.100489
7. Chen, Y., Gao, Y., & Guo, H. (2021). Bio-improved hydraulic properties of sand treated by soybean urease induced carbonate precipitation and its application Part 2: Sand-geotextile capillary barrier effect. Transp Geotech 27(September 2020), 100484. https://doi.org/10.1016/j.trgeo.2020.100484
8. Cheng L, Cord-Ruwisch R (2012) In situ soil cementation with ureolytic bacteria by surface percolation. Ecol Eng 42:64–72
9. Cheng L, Shahin MA, Mujah D (2017) Influence of key environmental conditions on microbially induced cementation for soil stabilization. J Geotech Geoenviron Eng 143(1):04016083
10. Cui M-J, Zheng J-J, Zhang R-J, Lai H-J, Zhang J (2017) Influence of cementation level on the strength behaviour of bio-cemented sand. Acta Geotech 12(5):971–986
11. DeJong JT, Fritzges MB, Nüsslein K (2006) Microbially induced cementation to control sand response to undrained shear. J Geotech Geoenviron Eng 132(11):1381–1392
12. DeJong JT, Mortensen BM, Martinez BC, Nelson DC (2010) Bio-mediated soil improvement. Ecol Eng 36(2):197–210

13. DeJong JT, Soga K, Kavazanjian E, Burns S, Van Paassen LA, Al Qabany A, Aydilek A, Bang SS, Burbank M, Caslake LF, Chen CY, Cheng X, Chu J, Ciurli S, Esnault-Filet A, Fauriel S, Hamdan N, Hata T, Inagaki Y, Jefferis S, Kuo M, Laloui L, Larrahondo J, Manning DAC, Martinez B, Montoya BM, Nelson DC, Palomino A, Renforth P, Santamarina JC, Seagren EA, Tanyu B, Tsesarsky M, Weaver T (2013) Biogeochemical processes and geotechnical applications: progress, opportunities and challenges. Géotechnique 63(4):287–301

14. Dhami NK, Reddy MS, Mukherjee A (2013) Biomineralization of calcium carbonates and their engineered applications: a review. Front Microbiol 4(October):314

15. Gomez MG, Martinez BC, DeJong JT, Hunt CE, deVlaming L, A., Major, David W., Dworatzek, Sandra M, (2015) Field-scale bio-cementation tests to improve sands. Ground Improvement 168(3):206–216

16. Jiang NJ, Soga K, Kuo M (2017) Microbially induced carbonate precipitation for seepage-induced internal erosion control in sand-clay mixtures. J Geotech Geoenviron Eng 143(3):04016100

17. Kim D H, Mahabadi N, Jang J and van Paassen L A (2020). Assessing the kinetics and pore-scale characteristics of biological calcium carbonate precipitation in porous media using a microfluidic chip experiment. Water Resour Res, 56, e2019WR025420.

18. Konstantinou C, Biscontin G (2021) Soil enhancement via microbially induced calcite precipitation. In: Geotechnical aspects of underground construction in soft ground. CRC Press, pp 765–772. https://doi.org/10.1201/9780429321559

19. Konstantinou C, Biscontin G, Jiang NJ, Soga K (2021) Application of microbially induced carbonate precipitation (MICP) to form bio-cemented artificial sandstone. J Rock Mech Geotech Eng. https://doi.org/10.1016/j.jrmge.2021.01.010

20. Konstantinou C, Wang Y, Biscontin G, Soga K (2021) The role of bacterial urease activity on the uniformity of carbonate precipitation profiles of bio-treated coarse sand specimens. Sci Rep 11:6161. https://doi.org/10.1038/s41598-021-85712-6

21. Konstantinou C, Biscontin G, Logothetis F (2021) Tensile strength of artificially cemented sandstone generated via microbially induced carbonate precipitation. Materials 14(16):4735. https://doi.org/10.3390/ma14164735

22. Lai HJ, Cui MJ, Wu SF, Yang Y, Chu J (2021) Retarding effect of concentration of cementation solution on biocementation of soil. Acta Geotech 16(5):1457–1472. https://doi.org/10.1007/s11440-021-01149-1

23. Lin H, Suleiman MT, Brown DG, Kavazanjian E Jr (2015) Mechanical behavior of sands treated by microbially induced carbonate precipitation. J Geotech Geoenviron Eng 142:04015066

24. Mahawish A, Bouazza A, Gates WP (2018) Improvement of coarse sand engineering properties by microbially induced calcite precipitation. Geomicrobiol J 35(10):887–897

25. Martinez BC, DeJong JT, Ginn TR, Montoya BM, Barkouki TH, Hunt C, Tanyu B, Major D (2013) Experimental optimization of microbial-induced carbonate precipitation for soil improvement. J Geotech Geoenviron Eng 139:587–598

26. Phillips AJ, Lauchnor E, Eldring J, Esposito R, Mitchell AC, Gerlach R, Spangler LH (2013) Potential CO$_2$ leakage reduction through biofilm-induced calcium carbonate precipitation. Environ Sci Technol 47(1):142–149

27. Terzis D, Bernier-Latmani R, Laloui L (2016) Fabric characteristics and mechanical response of bio-improved sand to various treatment conditions. Géotech Lett 69(1):50–57

28. Terzis D, Laloui L (2018) 3-D micro-architecture and mechanical response of soil cemented via microbial-induced calcite precipitation. Sci Rep 8(1):1416

29. Terzis, Dimitrios and Laloui, Lyesse. 2019. A decade of progress and turning points in the understanding of bio-improved soils: a review. Geomech Energy Environ 19: 100116.

30. van Paassen L (2009) Biogrout: ground improvement by microbially induced carbonate precipitation. PhD Thesis, Delft University of Technology.

31. van Paassen L, Ghose R, van der Linden TJM, van der StarWRL and van Loosdrecht MCM, (2010) Quantifying biomediated ground improvement by ureolysis: large-scale biogrout experiment. J Geotech Geoenviron Eng 136(12):1721–1728

32. Wang Y, Soga K, DeJong JT, Kabla A (2019) A microfluidic chip and its use in characterizing the particle-scale behaviour of microbial-induced carbonate precipitation (MICP). Géotechnique 69(12):1086–1094

33. Wang Y, Soga K, DeJong JT, Kabla A (2019) Microscale visualization of microbial-induced carbonate precipitation (MICP) processes. J Geotech Geoenviron Eng 145(9):04019045

34. Wang Y, Soga K and Jiang NJ (2017) Microbial induced carbonate precipitation (MICP): the case for microscale perspective. In: Proceedings of the 19th international conference on soil mechanics and geotechnical engineering, 1099–1102.

35. Wang Y, Soga K, DeJong JT and Kabla A. (2021) Forthcoming. Effects of bacterial density on growth rate and characteristics of microbial-induced CaCO$_3$ precipitates: a particle-scale experimental study. ASCE J Geotech Geoenviron Eng.https://doi.org/10.1016/(ASCE)GT.1943-5606.0002509

36. Weinhardt F, Class H, Vahid Dastjerdi S, Karadimitriou N, Lee D, Steeb H (2021) Experimental methods and imaging for enzymatically induced calcite precipitation in a microfluidic Cell. Water Resour Res 57(3):1–11. https://doi.org/10.1029/2020WR029361

37. Whiffin VS, van Paassen LA, Harkes MP (2007) Microbial carbonate precipitation as a soil improvementtechnique. Geomicrobiol J 24(5):417–423

38. Whitesides GM (2006) The origins and the future of microfluidics. Nature 442(7101):368–373

39. Xiao Y, He X, Wu W, Stuedlein AW, Evans TM, Chu J, Liu H, van Paassen LA, Wu H (2021) Kinetic biomineralization through microfluidic chip tests. Acta Geotech 16(10):3229–3237. https://doi.org/10.1007/s11440-021-01205-w

40. Zehner J, Røyne A, Sikorski P (2021) A sample cell for the study of enzyme-induced carbonate precipitation at the grain-scale and its implications for biocementation. Sci Rep 11(1):1–10. https://doi.org/10.1038/s41598-021-92235-7

41. Zehner J, Røyne A, Wentzel A, Sikorski P (2020) Microbial-induced calcium carbonate precipitation: an experimental toolbox forin situand real time investigation of micro-scale pH evolution. RSC Adv 10(35):20485–20493. https://doi.org/10.1039/d0ra03897k

42. Zhao Q, Li L, Li C, Li M, Amini F, Zhang H (2014) Factors affecting improvement of engineering properties of MICP-treated soil catalyzed by bacteria and urease. J Mater Civ Eng 26(12):04014094. https://doi.org/10.1061/(asce)mt.1943-5533.0001013

43. Zhou H, Xu S, Sun Z (2018) Real-time in situ observation of shear modulus evolution during Ostwald ripening of colloidal crystallization. J Cryst Growth 502(June):35–40